Origin and geodynamic relationships of the Late Miocene to Quaternary alkaline basalt volcanism in the Pannonian Basin, eastern-central Europe

Szabolcs Harangi[1,2], M. Éva Jankovics[1,3], Tamás Sági[1,2], Balázs Kiss[1,3], Réka Lukács[1,3], Ildikó Soós[1]

[1] MTA-ELTE Volcanology Research Group, Pázmány sétány 1/C, H-1117 Budapest, Hungary; e-mail: szabolcs.harangi@geology.elte.hu

[2] Department of Petrology and Geochemistry, Eötvös University, Pázmány sétány 1/C, H-1117 Budapest, Hungary

[3]Vulcano Research Group, Department of Mineralogy, Geochemistry and Petrology, University of Szeged, Egyetem utca 2, H-6722 Szeged, Hungary

Abstract

Alkaline basaltic volcanism has been taking place in the Carpathian-Pannonian Region since 11 Ma and the last eruptions occurred only at 100-500 ka. It resulted in scattered low-magma volume volcanic fields located mostly at the margins of the Pannonian basin. Many of the basalts have compositions close to those of the primitve magmas and therefore can be used to constrain the conditions of the magma generation. Low degree (2-3%) melting could occur in the convective asthenosphere within the garnet-spinel transition zone. Melting started at about 100 km depth and continued usually up to the base of the lithosphere. Thus, the final melting pressure could indicate the ambient lithosphere-asthenosphere boundary. The asthenospheric mantle source regions of the basalts were heterogeneous, presumably in small scale, and included either some water or pyroxenite/eclogite lithology in addition to the fertile to slightly depleted peridotite. Based on the prevailing estimated mantle potential temperature

(1300-1400^{o}C) along with number of further observations we exclude the existence of mantle plume or plume fingers beneath this region. Instead, we propose that plate tectonic processes controlled the magma generation. The Pannonian basin acted as a thin-spot after the 20-12 Ma syn-rift phase and provided suction in the sublithospheric mantle, generating asthenospheric flow from below the adjoining thick lithospheric domains. A near vertical upwelling along the steep lithosphere-asthenosphere boundary beneath the western and northern margin of the Pannonian basin could result in decompressional melting producing low-volume melts. The youngest basalt volcanic field (Perşani) in the region is inferred to have been formed due to the dragging effect of the descending lithospheric slab beneath the Vrancea zone that could result in narrow rupture at the base of the lithosphere. Continuation of the basaltic volcanism cannot be excluded as inferred from the still fusible condition of the asthenospheric mantle. This is reinforced by the detected low-velocity seismic anomalies in the upper mantle beneath the volcanic fields.

Keywords: basalt, spinel, Carpathian-Pannonian region, magma genesis, monogenetic volcanic field, asthenosphere flow

Introduction

Origin of the basaltic magmas in monogenetic volcanic fields is a key issue to understand the nature of low-magma-flux, episodic, but long lasting volcanic activity (Connor and Conway, 2000; Wang et al., 2002; Aldanmaz et al., 2006; Jung et al., 2006; 2012; Valentine and Perry, 2007; Blondes et al., 2008; Haase and Renno, 2008; Brenna et al., 2012; McGee et al., 2013). Each volcano in such volcanic system is considered to represent eruption of a discrete magma batch ascending rapidly from the mantle source, although recent studies revealed that composition of erupted magmas could change even within the eruptive sequence

of a monogenetic volcano (Strong and Wolff, 2003; Brenna et al., 2010; Erlund et al., 2010; McGee et al., 2012). Apart of these exceptions, basalts of monogenetic volcanoes provide a unique snapshot of the nature of the mantle source regions and could reveal their subtle compositional differences. Furthermore, basaltic products having composition close to the primitive magmas can be used to infer the condition of the mantle generation (pressure and temperature, mineral and chemical composition of the melted mantle rock, degree of melting, mixing of melts etc.). Using this knowledge, a better understanding can be achieved about the triggering mechanism of the melt generation and the geodynamic relationships of the volcanism. Nevertheless, recent studies have revealed that evolution of basaltic magmas could be far more complex than previously thought (Woodland and Jugo, 2007; Smith et al., 2008; Jankovics et al., 2012; 2013) and careful investigation is necessary to select the most appropriate samples, which can be used to gain insight into the mantle and the melting process.

The Carpathian-Pannonian region (CPR; Fig. 1.) is a key natural laboratory for studying the interaction of deep mantle processes, igneous activity and tectonic events (Szabó et al., 1992; Seghedi et al., 1998; 2004a; 2004b; 2005; Harangi, 2001a; Konečný et al., 2002; Harangi and Lenkey, 2007; Seghedi and Downes, 2011). Alkaline basalt monogenetic volcanic fields have developed since 11 Ma, partly overlapping and partly postdating the extensive calc-alkaline andesitic-dacitic volcanism (Pécskay et al., 2006; Lexa et al., 2010). The alkaline basaltic volcanism is considered as part of the widespread Neogene to Quaternary volcanism in western and central Europe (Wilson and Downes, 1991; 2006; Embey-Isztin and Dobosi, 1995; Lustrino and Wilson, 2007), but it shows many similarities also with the alkaline basaltic volcanism occurred with close spatial and temporal association of calc-alkaline and potassic-ultrapotassic volcanism in the Mediterranean (Wilson and Bianchini, 1999; Harangi et al., 2006; Beccaluva et al., 2011). The origin of the basaltic

volcanism in the CPR is still controversial (Embey-Isztin and Dobosi, 1995; Embey-Isztin et al., 2001; Harangi, 2001a; 2001b; Seghedi et al., 2004a; Harangi and Lenkey, 2007; Ali and Ntaflos, 2011; Ali et al., 2013; Harangi et al., 2013), largely due to its occurrence after the main extensional phase of the Pannonian basin. Eruption of basaltic magmas took place even at a couple of 100's ka, thus, understanding the mechanism of melt generation is crucial also to evaluate rigorously whether this kind of volcanic activity could continue in the future.

In this paper, we discuss the conditions of the basaltic magma generation in the CPR using primarily those samples, which have chemical composition close to primitive magmas. We combine major and trace element data of the host basalts as well as compositional features of spinels, one of the liquidus minerals in these rocks, to constrain the origin of the magmas and the nature of the source regions. Then, we propose a possible mechanism that could be responsible for the formations of the basaltic volcanoes in this region.

Geological setting

The Carpathian-Pannonian region lies in the northeastern part of the Alpine-Mediterranean region and is characterized by an arcuate orogenic belt (Carpathians) with a basin area behind it (the Pannonian basin; Fig. 1A). The Pannonian basin is surrounded by the Alpine, Carpathian and Dinarides mountain belts. It is underlain by thin lithosphere (50-80 km) and crust (22-30 km) coupled with high heat flow (>80 mW/m^2; Csontos et al., 1992; Horváth, 1993; Tari et al., 1999; Lenkey et al., 2002; Horváth et al., 2006). It is regarded as a special type of back-arc basin formed by heterogeneous stretching of the lithosphere. The thinning of the lithosphere started in the Early Miocene (around 20 Ma) and the syn-rift phase was finished by the end of Miocene (around 12 Ma; Horváth et al., 2006). Tari et al. (1999) defined an initial core-complex style extension during the Early Miocene followed by a wide-

rift type extension. Huismans et al. (2001) distinguished two main rifting events, involving a Middle Miocene passive rifting followed by a Late Miocene active rifting episode. As a consequence, the lithospheric mantle underwent a dramatic attenuation (stretching factor of 5–50), whereas the crust was only moderately thinned (stretching factor of 1.2–2.5) leading to the suggestion of an inhomogeneous stretching model (Sclater et al., 1980; Horváth et al., 1988; 2006). As an extreme case, Horváth et al. (2006) assumed the disappearance of the whole mantle lithosphere beneath the Pannonian Basin at the beginning of the synrift phase. The thinning of the lithosphere was accompanied by asthenospheric mantle updoming as shallow as 50-60 km (Stegena et al., 1975; Huismans et al., 2001; Konečný et al., 2002) and therefore, the Pannonian basin can be considered as one of the hottest basin areas of Europe (Cloetingh et al., 2007). The syn-rift phase was followed by post-rift thermal subsidence, when several thousands meters of Late Miocene to Quaternary sediments filled parts of the basin areas (Great Hungarian Plain, Little Hungarian Plain).

There are diverse views on the driving mechanism of the lithospheric extension such as (a) formation of an overthickened hot lithosphere, which underwent gravitational collapse during the Early Miocene (Tari et al., 1999; Horváth et al., 2006); (b) suction of the slab roll-back beneath the retreating subduction along the Eastern Carpathians (Csontos et al., 1992); (c) dripping the lower, gravitationally instable lithospheric material into the deep mantle (Lorinczi and Houseman, 2000) and (d) asthenospheric flow either via the "Istria window" beneath the Dinarides (Horváth and Faccenna, 2011) or from the Adria–European collision zone and ensuing Alpine orogeny (Kovács et al., 2012). While the models (a) and (b) are supported by geophysical and geological observations and are widely accepted by the scientific community, the novel models (c) and (d) have still a number of inconsistencies and therefore need more supporting evidences.

Since the Pliocene, the CPR has been in a tectonic inversion stage (Horváth and Cloetingh, 1996; Bada et al., 1999) due to the continuous push from west (Adria-push from the Alps–Dinarides belt) and blocking the area at east by the thick Ukrainian lithosphere. The entire basin system has been landlocked and this led to a gradual structural inversion in the form of multi-scale folding and fault reactivation. Some parts of the CPR (Great Hungarian Plain, Little Hungarian Plain and Danube basin, Vienna basin, Styrian basin and Brasov basin) are still subsiding, while other parts show uplift (Dombrádi et al., 2010). This differential vertical movement is accommodated by reactivation of older faults. Major strike-slip faults have a SW-NE orientation at the northern and central part of the CPR, whereas to the south a characteristic E-W trending strike-slip fault system was identified (Horváth et al., 2006; Fig. 1B).

The nature of the upper mantle beneath the CPR is inferred from seismic tomographic models. These show a high-velocity body in the transition zone (400-670 km) interpreted as accumulated subducted slab material (Wortel and Spakman, 2000; Piromallo and Morelli, 2003; Hetényi et al., 2009), a near-vertical high-velocity slab beneath the southeastern margin of the CPR (Vrancea zone), regarded as the trace of final-stage subduction (Sperner et al., 2001; 2004) and relatively low velocity material between the transition zone and the base of lithosphere.

Areal distribution of the basalts

In the CPR, four main monogenetic volcanic fields were developed (Styrian, Bakony-Balaton Upland, Nógrád-Gemer, Perşani; Fig. 1B). In addition, localized basaltic centres were developed in a few areas (Pauliberg-Oberpullendorf in Burgenland, Lucaret-Sanovita in Banat), where no precursor and subsequent volcanism occurred. Basalt volcanic centres of the

150 eastern part of the Little Hungarian Plain (called here Kemenes Volcanic Field, Fig. 1B) and
151 around Štiavnica (ST in Fig. 1B) can be considered to form ultra-low-magma-flux volcanic
152 fields, where volcanic activity was sporadic (<10 volcanic centres) during a considerable (2-6
153 Myr) timescale and characterized by several 100's ka (several Myr in ST) long quiescence
154 time between the active events.

155 The basaltic volcanism was controlled by external conditions, such as tectonics,
156 topography, presence and style of aquifer in the basement (Martin and Németh, 2004;
157 Kereszturi et al., 2011). Tuff rings and maar structures were developed as a result of
158 phreatomagmatic explosive eruptions followed occasionally by pure magmatic explosive
159 volcanism and in a few cases lava lakes were formed in the late-stage effusive phase. Large
160 volcanic edifices, such as shield volcanoes were built up in each volcanic field (Stradner
161 Kogel in Styria, Kab, Agár and Fekete hills in the Bakony-Balaton Upland, Medvedia in
162 Nógrád-Gemer) except for the Perşani. The volcanism was dominantly basaltic, the only
163 exception is the Kemenes Volcanic Field, where a large trachyandesite-trachyte volcano
164 developed around 10-11 Ma (Pásztori volcano; Harangi et al., 1995; Harangi, 2001b). This
165 volcano subsided subsequently and was covered by thick (over 2000 m) Late Miocene to
166 Quaternary sediments.

167 The geographic location of the volcanic fields in the CPR (Fig. 1B) is remarkable,
168 since they are mostly at the western and northern margins of the Pannonian basin and not in
169 the central area, where there is the thinnest lithosphere, whereas the youngest one is found at
170 the southeastern part of the region, close to the seismically active Vrancea zone. The two
171 largest volcanic fields in the CPR are the Bakony-Balaton Upland Volcanic Field (Martin and
172 Németh, 2004) and the Nógrád-Gemer Volcanic Field (Konečný et al., 1995; 1999), each of
173 them involves about 50 eruptive centres, have relatively long timescale of the volcanism (6-8
174 Ma) and includes intermittent active phases with relatively long (several 100's ka) repose

175 time. Kereszturi et al. (2011; 2013) calculated the recurrence rate for both volcanic fields and
176 got about 0.11 and 0.08 Ma/event, respectively. Although the volcanic edifices are deeply
177 eroded in both areas, they estimated also the magma-flux that is 0.9 km^3/Ma (calculated only
178 for the last 5 active phases, excluding the initial phase) and 0.4 km^3/Ma, respectively (the total
179 erupted magma volume is estimated to be about 4 and 3.5 km^3, respectively). These numbers
180 are comparable with the low magma-flux monogenetic volcanic fields, such as the
181 Southwestern Nevada Volcanic Field (Valentine and Perry, 2007) and classify them as typical
182 tectonically-controlled, time predictive volcanic fields. The Styrian and Perşani Volcanic
183 Fields (Seghedi and Szakács, 1994; Downes et al., 1995; Ali and Ntaflos, 2013; Harangi et al.,
184 2013) contain less eruptive centres, although in Styria, the eruptive volume could be relatively
185 large (>1 km^3 total volume) due to the significant amount of effusive volcanic products
186 (Stradner Kogel, Klöch, Steinberg). The Perşani Volcanic Field is the youngest one in the
187 CPR and is located in a 22 km long and 8 km wide area (Seghedi and Szakács, 1994) at the
188 northwestern periphery of the intramontane Braşov basin (Fig. 1B.). This area is characterized
189 by NE-SW trending normal faults, resulting from a NW-SE extensional regime (Gîrbacea et
190 al., 1998). The eruptive centres appear to be structurally controlled and show a rough NE-SW
191 trending alignment. Popa et al. (2012) recorded subcrustal seismicity beneath the Perşani area
192 and, using seismic tomography modelling, suggested that a low-velocity anomaly could be
193 inferred at the crust-mantle boundary. The youngest basalt volcano (Putikov vŕšok; Šimon and
194 Halouzka, 1996) of the CPR is located near Banska Štiavnica upon the Late Pleistocene
195 terrace of the river Hron. It does not rigorously belong to the Nógrád-Gemer Volcanic Field
196 and was formed after more than 6 Ma quiescence in this area. There are two ‘satellite
197 volcanoes” in the CPR: The alkaline basalts of Pauliberg and Oberpullendorf are found at the
198 Alps-Pannonian Basin transition zone in Burgenland (Harangi, 2001b; Ali and Ntaflos, 2011)
199 and represent a single volcanic episode at about 11 Ma. Harangi et al. (1995) suggested that

200 they could have some compositional similarities with the basaltic dyke rocks in the Pásztori
201 volcano. In the southern part of the CPR, the alkaline basalt of the Lucaret-Sanovita belongs
202 also to a single eruptive event without any precursor magmatism. It is located close to a major
203 west-east trending strike-slip zone (Fig. 1B) and at the boundary of subsiding and uplifting
204 areas (Dombrádi et al., 2010). Remarkably, further single – potassic-ultrapotassic - volcanoes
205 (Bár, Uroi) were formed also along this tectonic line during the last 2.5 Ma.
206
207 **Temporal evolution**
208
209 Monogenetic basalt volcanic fields are typically active over millions of years. The
210 volcanism is characterized by intermittent eruptions gathering often in active phases, which
211 are separated by long repose periods. Recurrence rate of volcanism is particularly important in
212 evaluating the volcanic hazard (Condit and Connor, 1996; Valentine and Perry, 2007),
213 although precise dating of eruptions is difficult for basaltic rocks. In the Pannonian Basin,
214 eruption ages were determined mostly by K/Ar radiometric technique (Balogh et al., 1982;
215 1986; 1990; 1994; Borsy et al., 1986). Ar/Ar dating was performed for the basaltic rocks of
216 the Bakony-Balaton Upland volcanic fields that corroborated the reliability of the former
217 K/Ar data (Wijbrans et al., 2007). In contrast, the new Ar/Ar age data (Panaiotu et al., 2013)
218 refined significantly the former knowledge (Panaiotu et al., 2004) on the temporal evolution
219 of the Perşani volcanic field. So far, the available K/Ar data base provides a solid framework
220 for the temporal evolution of the alkaline basaltic volcanism in the Pannonian basin, although
221 more careful studies are necessary to define the recurrence rates in individual volcanic fields
222 more precisely and constrain the eruption age of the youngest volcanic episodes.
223 In the Pannonian Basin, eruption of alkali basaltic magmas started in the westernmost
224 margin, where two outcrops are known, at Pauliberg and at Oberpullendorf in Burgenland

225 (Ali and Ntaflos 2011) and their ages were determined as 11.7 to 10.5 Ma (Balogh et al.,
226 1994). Similar ages were published for the basalts found in drilling cores around Kecel
227 (central Pannonian basin; 8.1-10.4 Ma; Balázs and Nusszer 1987). Although these basalts are
228 strongly altered, their Late Miocene ages were corroborated by stratigraphic data.
229 The basaltic volcanism in the two largest volcanic fields (Bakony-Balaton Upland and
230 Nógrád-Gemer) lasted for more than 6 Myr. Noteworthy, eruption of basaltic magmas in both
231 areas commenced at 7.8-8.0 Ma (Balogh and Németh, 2005; Balogh et al., 2005; Chernyshev
232 et al., 2013) and continued after 2 Ma quiescence in the Bakony-Balaton Upland and after
233 about 1 Ma repose time in the Nógrád-Gemer area. The volcanism in both areas was
234 characterized by closely packed active phases separated by long repose periods (Konečný et
235 al., 1995; 1999; Wijbrans et al., 2007). Kereszturi et al. (2013) estimated the peak magma
236 output times being at 3-4 Ma in the Bakony-Balaton Upland volcanic field and 1.5-3.0 Ma in
237 the Nógrád-Gemer area. The alkaline basalt occurrences cropping out within the area of the
238 Middle Miocene eroded andesitic Štiavnica composite volcanic complex are spatially
239 separated from the Nógrád-Gemer volcanic field. They show highly sporadic eruption times,
240 such as 6.6-7.8 Ma in Banska Štiavnica and Dobrá Niva and 0.1-0.5 Ma for the Putikov
241 volcano at the Hron river (Balogh et al., 1981; Konečný et al., 1999; Šimon and Halouzka,
242 1996; Šimon and Maglay, 2005; Chernyshev et al., 2013). The age of the Putikov vŕšok
243 volcano has a particular importance, since it indicates the latest alkaline basalt eruption in the
244 CPR. Balogh et al. (1981) and later, Chernyshev et al. (2013) provided 430-530 ka eruption
245 ages using K/Ar technique, whereas Šimon and Halouzka (1996) considered the stratigraphic
246 position of the lava flow and interpreted it as sitting on the Late Pleistocene (Riss) terrace of
247 the Hron river and this points to an age of 120-150 ka. This younger age was supported by
248 optically stimulated luminescence (OSL) dating of the underlying sediments that yielded an
249 age of 102± 11 ka. Further investigation is necessary and highly important to constrain the

exact eruption age of this basalt. The youngest eruption ages in the Nógrád-Gemer volcanic field require also detailed investigation. In the last intense eruptive phase between 1.1-1.5 Ma, mostly effusive activity was recognized (Konečný et al. 1995; 1999). The latest eruptions in this area was previously thought to have occurred around 400 ka (Hodejov and Fil'akovo maars; Konečný et al. 1995), however, new (U-Th)/He zircon dating (Hurai et al., 2013) did not confirm this young age.

In the western margin of the CPR (Styrian basin; Ali et al., 2013), alkaline basaltic volcanism occurred between 3.9 and 1.9 Ma (Balogh et al., 1994) after a long quiescence period since the 14.0-17.5 Ma high-K trachyandesitic volcanic activity (Harangi et al., 1995). The latest eruption resulted in a relatively large volume shield volcano composed of nephelinites at Stradner Kogel.

The youngest monogenetic volcanic field of the CPR is located at the western margin of the Perşani Mts., between the Transylvanian basin and the Brasov basin (Seghedi and Szakács, 1994; Downes et al., 1995; Harangi et al., 2013). Although former K/Ar and palaeomagnetic dating (Panaiotu et al., 2004) implied two, well separated eruption phases, the new Ar/Ar dating (Panaiotu et al., 2013) revised this and indicated a fairly continuous, but very scattered volcanism from 1.22 Ma to 0.52 Ma.

Finally, a unique basalt occurrence is found at Lucaret (southern Pannonian basin), where no precursor volcanic activity took place and the age of this basalt was determined as 2.4 Ma (Downes et al., 1995).

Petrologic and geochemical characteristics

Petrologic and geochemical features of the alkaline basaltic rocks of the CPR have been published in several papers (Embey-Isztin et al., 1993; 2001; Seghedi and Szakács,

1994; Dobosi et al., 1995; Downes et al., 1995; Harangi et al., 1995; 2013; Harangi, 2001b; Harangi and Lenkey, 2007; Ali and Ntaflos, 2011; Tschegg et al., 2010; Jankovics et al., 2012; 2013; Ali et al., 2013) and we completed them with new analysis, mostly from the Nógrád-Gemer Volcanic Field (Sági et al., 2013). Representative composition of the basalts from different locations is given in Table 1. In this section, we provide a brief summary on the main features of the basalts.

The basaltic rocks are classified as alkali basalts, trachybasalts, basanite, phonotephrite and nephelinite (Fig. 2). Evolved rocks types occur in the buried Pásztori volcano, they are trachyandesite and trachyte (Harangi et al., 1995; Harangi, 2001b). Most of the basalts are olivine-phyric, while clinopyroxene phenocryst is found in a few localities of the Bakony-Balaton Upland and Kemenes Volcanic Field, but is more common in the basalts of the Styrian Volcanic Field and in the Nógrád-Gemer Volcanic Field. The olivine phenocrysts with Fo>84 mol% often contain spinel inclusions and these two minerals can be regarded as liquidus phases. Both minerals have a wide compositional range (Embey-Isztin et al., 2007; Ali and Ntaflos, 2011; Jankovics et al., 2012; 2013; Ali et al., 2013; Harangi et al., 2013). The most magnesian olivines have typically high Mn content compared with the trend defined by Herzberg (2011) for olivines crystallized from peridotite-derived magmas. They are characterized by low Fe/Mn ratio (Fe/Mn=40-75); this feature along with the relatively low Ni content (<2500 ppm) is not consistent with derivation of the primary magmas from pyroxenite source as defined by Sobolev et al. (2007) and Herzberg (2011). Clinopyroxene phenocrysts could have crystallized mostly at the crust mantle boundary zone as shown by the geobarometric calculations. Their complex zoning often found in basalts from the Nógrád-Gemer and the Bakony-Balaton Upland indicates mixing of magma batches at depth (Dobosi, 1989; Dobosi and Fodor, 1992). Mantle-derived ultramafic and lower crustal granulite

299 xenoliths are common in basalts of each volcanic field (Embey-Isztin et al., 2001; Szabó et
300 al., 2004).
301 The CPR basalts are almost exclusively silica-undersaturated and have mg-numbers
302 ranging from 0.5 to 0.8 (MgO=5-15 wt%). The most magnesian basalts contain, however,
303 significant amount of xenocrysts (e.g., Bondoró and Füzes at Bakony-Balaton Upland), which
304 strongly modify the bulk rock composition (Jankovics et al., 2012; 2013). Majority of the
305 basalts have an mg-number >0.62 suggesting only a minor to moderate effect of fractional
306 crystallization. Moderately fractionated basalts are found mostly in Styria and in the Nógrád-
307 Gemer areas. For this study, we selected those samples that have mg-number between 0.64
308 and 0.72 (MgO=8-13 wt%) and therefore their compositions are close to that of the primitive
309 magmas. In these samples, variation of major elements indicates the controlling factor of
310 various amounts of olivine fractionation. However, characteristic differences can be
311 recognized between the most primitive basalts. The Pauliberg basanite has a distinct
312 composition with low Al_2O_3 and high TiO_2 and FeO contents (Fig. 3). Experimental studies
313 suggest that such composition could be obtained by low-degree melting of carbonated, silica-
314 deficient eclogite (Dasgupta et al., 2006; Kogiso and Hirschmann, 2006). The basalts from
315 Oberpullendorf (Burgenland) and Putikov vŕšok (Štiavnica) have a transitional major element
316 composition between the Pauliberg basanite and the rest of the CPR basalts.
317 The trace element composition of basalts resembles those commonly found in intra-
318 plate magmas and is similar to the Neogene to Quaternary alkaline mafic rocks in Western
319 and Central Europe (Wilson and Downes, 1991; Lustrino and Wilson, 2007). The FTS
320 elements, such as Ni, Cr and Sc have relatively high abundances (Ni=100-300 ppm; Cr=100-
321 500 ppm; Sc=10-30 ppm; Fig. 3) consistent with the slight olivine±spinel-dominated
322 fractional crystallization. Based on the primitive mantle (McDonough and Sun, 1995)
323 normalized trace element patterns, Harangi and Lenkey (2007) defined two main

compositional groups: the first one is characterized by stronger enrichment in incompatible trace elements and a typical negative potassium anomaly, whereas the second one has smoother trace element patterns and no negative potassium anomaly (Fig. 4). The strongly incompatible trace elements have a wide compositional range (La=25-90 ppm, Nb=30-130 ppm, Th=3-13 ppm; Fig. 3) and show a positive correlation with an intercept of zero. Same covariance with Ba can be also observed although the basalts from Pauliberg and Styria show a distinct trend.

Sr-Nd-Pb isotope ratios of the basalts were published by Embey-Isztin et al. (1993), Dobosi et al. (1995), Downes et al. (1995) and Harangi et al. (1995). All of the basalts fall into the depleted field in Sr-Nd isotope space, similarly to majority of the Neogene to Quaternary alkaline mafic rocks in Western and Central Europe (Wilson and Downes, 1991; Wilson and Patterson, 2001). The most depleted end-member of this variation trend is a mixture of HIMU and DMM. In the Pb-Pb isotopic diagrams, they show a relatively large variation, many of the samples have relatively high $^{207}Pb/^{204}Pb$ ratio (>15.6) causing a vertical shift from the NHRL. The highest $^{206}Pb/^{204}Pb$ ratio (19.6-19.7) is shown by the Pauliberg basanite.

Discussion

Most of the alkaline basalts of the CPR show chemical composition (MgO>8 wt%; Ni=130-350 ppm; Fig. 3) that could be close to that of the primitive magmas. Using only these samples, the condition of the melting process as well as the nature of the source region can be constrained that could contribute to our understanding on the reason of mantle melting beneath the area. Trace element ratios such as Nb/Th (5–15) and Nb/La (1–2) of the basalts show values that are higher than those observed in continental crustal rocks (Rudnick and

Fountain, 1995) and are typical of mantle-derived melts, mostly for those derived from the asthenosphere. Therefore, we can conclude that crustal contamination did not significantly modify the trace element composition of the CPR mafic magmas. Most of the selected basalts are olivine-phyric and the olivine phenocrysts often contain spinel inclusions indicating that these mineral phases could have been liquidus minerals as have been suggested for the usual evolution of alkaline silica-undersaturated mafic magmas (Roeder et al., 2006). High pressure clinopyroxene crystallization could modify the magma composition as well as the composition of coexisting evolving phases and this should be considered even in the absence of clinopyroxene phenocrysts in the rocks (Smith et al., 2008). This would decrease the CaO content of the magma and possibly also leads to lowering the CaO content of the olivine phenocrysts. Nevertheless, our geothermobarometric calculations on selected clinopyroxenes in some basalts (Harangi et al., 2013) suggest that they crystallized later then the olivines. The relatively high Sc content of the basalts (Sc>15 ppm except for the samples from Lucaret) and the uniform Cr-number of the spinels along with various Fo content of coexisting olivines also imply that no significant early-stage clinopyroxene fractionation occurred that would significantly modify the magma composition. Taking all of this into account, the composition of the alkaline basalts with MgO>8 wt% can be used to infer the melting condition and the nature of the source rock.

In this discussion, we attempt to constrain the origin of the magmas using the following principle: we consider the simplest model over the complex models and take a complex model only when no simple model works (Niu, 2005). Thus, we simplified the mantle source material considering to be dominantly peridotitic in lithology, knowing, however, that involvement of more fusible material, such as pyroxenite or eclogite could be possible. There are some inferences for the existence of such material in the mantle source

region, but we think that further, careful investigation is necessary to test their influence on the melting models and the composition of the primary magmas.

Asthenospheric vs. lithospheric mantle source region

Origin of the continental intraplate basaltic rocks is often debated. Alkaline silica-undersaturated mafic magmas are considered being generated by low-degree of melting either in the upwelling asthenosphere (Bradshaw et al., 1993; Wang et al., 2002; Niu et al., 2011; Gazel et al., 2012) or by melting of metasomatic, usually amphibole-rich veins in the lithosphere (Fitton et al., 1991; Ormerod et al., 1991; DePaolo and Daley, 2000; Beccaluva et al., 2007; Valentine and Perry, 2007; Bianchini et al., 2008; Pilet et al., 2008; Mayer et al., 2013; 2014). Variation of trace element and isotopic compositions of the Neogene to Quaternary basaltic rocks in Europe led Wilson and Downes (1991; 2006) to conclude that both mantle regions could have contributed to the magma generation. This was reinforced by the more specific studies in various parts of volcanic areas in Europe (Haase et al., 2004; Haase and Renno, 2008; Jung et al., 2012), including the Pannonian basin (Embey-Isztin and Dobosi, 1995; Harangi, 2001a; Seghedi et al., 2004) and was suggested also for the origin of the basaltic magmas in the western USA (Fitton et al., 1988; 1991), in the Auckland volcanic field, New Zealand (McGee et al., 2013) and western Syria (Ma et al., 2011). However, an important question is why the colder lithospheric mantle undergoes melting. For this, the presence of fusible material (metasomatic veins) and either significant thinning of the lithosphere or a thermal perturbation (heating) are necessary. The fusible material is usually considered to be amphibole-bearing veins, which originated from low-volume asthenospheric melts and are frozen in the lower lithosphere (McKenzie, 1989; Niu, 2008; Pilet et al. 2008; Humphreys and Niu, 2009). The presence of amphibole in the source region is usually

inferred based on the negative K-anomaly in the primitive mantle normalized trace element patterns (Class and Goldstein, 1997; Späth et al., 2001; Jung et al., 2005; Haase and Renno, 2008). Amphibole is stable up to about 1100^{o}C temperature and up to about 2.5-3.0 GPa (ca. 100 km depth) and is regarded to be confined to the lithospheric mantle (Wallace and Green, 1991).

The negative K-anomaly as expressed by the K/K* ratio (calculated as $K_N/\sqrt{(Nb_N*La_N)}$, where K_N, Nb_N and La_N are primitive mantle normalized values) is a characteristic feature of many of the CPR basalts and shows a wide continuous range (K/K*=0.3-1.2; Fig. 5). It has a negative correlation with the La/Y and $(Sm/Yb)_N$ ratios, which are the indicators of the degree and the relative depth of melting. This could suggest that a K-bearing phase, presumably amphibole was present in the source of all of the CPR magmas and remained in the residual mantle during low degree melting and entered into the melt in the case of larger melting. In that situation, the source of the magmas should be entirely the lithospheric mantle. Melting of the lower lithosphere in the post-rift phase of the Pannonian basin cannot be explained by decompression-driven process, but only by thermal perturbation, i.e. via heat flux from the underlying asthenospheric mantle. Taking this view, Seghedi et al. (2004b) postulated localized mantle plumes (plume fingers) beneath the basalt volcanic fields of the CPR. However, there is lack of physical evidences for the generation of localized hot mantle upwelling scattered beneath the Carpathian-Pannonian region and there is a lack of explanation why this does not occur beneath the central Pannonian basin, where there is the thinnest lithosphere. Furthermore, the lowest K/K* value is shown by the basalts having the highest $(Sm/Yb)_N$ ratios and therefore reflect garnet in the source region. This would mean melting at depth greater than 80 km, which is already the asthenospheric mantle beneath most part of the region. Nevertheless, theoretically, it is possible that the high $(Sm/Yb)_N$ ratio is inherited in the metasomatic vein (Pilet et al., 2008). Although Pilet et al.

(2008) claimed that preferential melting of this material would yield magma composition akin to alkaline mafic magmas, others suggest that in this case potassic magmas are generated (McKenzie, 1989; Wilson and Downes, 1991; Cebriá and López-Ruiz, 1995). Furthermore, the K/K* ratio in the CPR basalts has no correlation with the La/Nb ratio that is used as an indicator of the lithospheric mantle (Fitton et al., 1991). In addition, the La/Nb ratio of the CPR basalts is less than 1 which is characteristic of asthenosphere-derived magmas. Finally, many alkaline OIB, such as St. Helena-type basalts (Chaffey et al., 1989; Kawabata et al., 2011) show negative K-anomalies, typically those formed by low-degree melting. Although, melting of metasomatized lithosphere cannot be excluded as a potential origin of such basalts (Pilet et al., 2005; 2008), most authors consider them as derived from upwelling hot mantle beneath the oceanic lithosphere. Thus, this compositional feature could be rather general both in oceanic and continental realms and could be an inheritance in the mantle source regions, possibly representing the most fusible part (eclogite or pyroxenite with negative K-anomaly and HIMU/FOZO characteristics; Sobolev et al., 2005; 2007; Fekiacova et al., 2007; Dasgupta et al., 2010; Timm et al., 2009) of the melted mantle material. In this context, it is noteworthy, that a correlation between the K/K* value and the radiogenic isotope ratios ($^{87}Sr/^{86}Sr$ and $^{143}Nd/^{144}Nd$; Fig. 5) is observed within the volcanic fields and that can be more readily explained by derivation of the magmas with compositionally distinct mantle sources. Lower degrees of melting would produce magmas from the more fusible parts of the source region that are characterized by low $^{87}Sr/^{86}Sr$ and high $^{143}Nd/^{144}Nd$ isotope ratios similar to HIMU/FOZO (Stracke et al., 2005) and negative K-anomaly (low K/K*), whereas higher degree of melting would lead to mixing with melts coming from compositionally distinct mantle domains (Harangi and Lenkey, 2007).

In summary, derivation of the basaltic magmas solely from the lithospheric mantle does not seem to be a plausible model in the CPR. In turn, we suggest that composition of the

448 CPR basalts is consistent with melting predominantly or even entirely of the asthenospheric
449 mantle. Since there are no convincing evidences for the existence of mantle plume or plume
450 fingers beneath this region, nor progressive lithospheric extension, we think that it is
451 physically difficult to generate significant amount of alkaline sodic magmas in the lithosphere
452 during the post-rift and tectonic inversion stages unless considering local detachment and
453 sinking of lithospheric fragments into the asthenosphere (Timm et al., 2010). At this stage, we
454 think that composition of the CPR basaltic rocks reflects mostly the nature of the source
455 region of the asthenospheric mantle and the heterogeneity within it.
456
457 ***Constrains on melting columns***
458
459 Considering that the basaltic magmas in the CPR could derive predominantly from the
460 asthenospheric mantle, an upward mantle flow is required to initiate melting. As the solid
461 mantle material moves upwards adiabatically, melting starts when the ambient temperature
462 intersects the solidus (initial melting pressure; Langmuir et al., 1992). This depth depends on
463 the mantle potential temperature as well as the nature of the mantle material (Langmuir and
464 Forsyth, 2007), but for alkaline mafic magmas it is usually within the garnet stability field, i.e.
465 deeper than 80 km (Niu et al., 2011). Melt production continues during further upwelling and
466 as a result, the initial magma composition will change due to the increasing extent of melting
467 and according to the changing mineral assemblage of the melted mantle rocks (from garnet to
468 spinel). Thus, the early-stage melt shows strong garnet-signature (high Ce/Y, Nb/Y and
469 $[Sm/Yb]_N$ ratios; Ellam, 1992; Salters and Hart; 1989; Putirka, 1999; Niu et al., 2011), but it
470 becomes progressively diluted in the strongly incompatible elements and looses their garnet
471 fingerprint. The extent of the melting column (defined by the initial and final melting
472 pressure, denoted as p_o and p_f, respectively) depends primarily on the thickness of the

lithosphere (Ellam, 1992; Langmuir et al., 1992; Haase, 1996; Putirka, 1999; Niu et al., 2011). Melting beneath thick lithosphere stops at greater depth and therefore produces smaller amount of magma, which are enriched in strongly incompatible trace elements and have a pronounced garnet-signature, whereas in areas where the lithosphere is thinner, melting could continue even in the spinel-stability field and produces more melt with different incompatible element abundances. Thus, the p_f can be used as a proxy for the thickness of the lithosphere, i.e. defining the depth of the lithosphere-asthenosphere boundary (LAB).

The pressure of the melting can be constrained by various methods. Major element composition of the primitive magmas is influenced by the pressure of melting and the extent of melting (Takahashi and Kushiro, 1983; Langmuir et al., 1992; Hirose and Kushiro, 1993; Baker and Stolper, 1994; Walter, 1998; Niu et al., 2011). MgO and FeO^t increase, SiO_2 decreases with increasing pressure of melting, whereas the Na_2O content of the primary magma depends mostly on the degree of melting. The CPR basalts have a relatively wide range of FeO content (FeO^t=8-12 wt%; Fig. 3) showing an inverse correlation with SiO_2 indicating that the primary magmas could have formed at various pressures. In order to quantify the pressure of melting, i.e. the depth of the magma generation first, correction of fractional crystallization has to be performed. This can be achieved by adding as much olivine to the bulk rock composition until the mg-number is around 0.72, consistent with a primitive melt composition that is in equilibrium with a melted peridotite with olivine having Fo-content around 0.9 mol%. For the selected mafic rocks of the CPR, correction of 5-15% olivine fractionation was necessary.

Langmuir et al. (1992) developed a model where the FeO^t and Na_2O contents of the primary magmas are used to constrain the intitial and final pressure of melting. Although this was constructed for mid-ocean ridge basalts, Wang et al. (2002) demonstrated that it provides reliable results for most melting within the depth interval of 50 and 110 km. The melting

498 model lines were compared with experimentally determined peridotite melts and a good
499 reproduction was obtained between 1.0 and 4.0 GPa. Furthermore, Wang et al. (2002)
500 emphasized that for magmas having Na_2O>3 wt% that is relevant for the CPR basalts, the
501 model is not dependant upon the melt pooling mechanism. We used this model calculation,
502 considering accumulated fractional melting process to determine the melting columns under
503 the alkaline basalt volcanic field of the CPR. In the Fig. 6A, each curve represents a different
504 initial melting pressure, i.e. where the ambient mantle temperature intersects the solidus. The
505 total iron content of the magma reflects the condition of the onset of melting, i.e. the initial
506 pressure that has a close relationship also with the mantle temperature. As melting proceeds,
507 the volume of magma increases and as a consequence the concentration of incompatible
508 elements as well as Na_2O decreases, while the total iron concentration does not change
509 significantly. Therefore, the final values of the FeO^t and the Na_2O of the accumulated melt
510 yield information on the initial melting pressure and the cessation of the melting, i.e. the final
511 melting pressure. These pressure values are then converted to depth, assuming average
512 densities of crust and mantle, 2.85 g/cm^3 and 3.25 g/cm^3, respectively as suggested by Wang
513 et al. (2002). The crustal thickness was taken as 32 km beneath Burgenland (western CPR)
514 and 35 km beneath Perşani (eastern CPR), whereas 28 km was used for the rest of the areas.
515 Note that the pressure/depth estimate has an about 10-20 km uncertainty due to various effects
516 such as the estimate of the primary composition, mantle fertility and the neglecting Fe^{3+} in the
517 iron content of the primitive melts (Wang et al., 2002).
518 We obtained p_o and p_f values for 13 basalt localities that cover all the monogenetic
519 volcanic fields of the CPR (Fig. 6A). Within them, only one basalt group from the Nógrád-
520 Gemer Volcanic Field shows a melting column with a depth interval that seems to be
521 unusually shallow (2.0 to 1.55 GPa, i.e. melting between 66 and 52 km). In all other cases the
522 initial and final melting pressure values are greater then 2 GPa; thus, considering the

lithospheric thickness beneath the Pannonoan basin, they indicate magma generation in the sublithospheric mantle. Generation of the primary magmas started predominantly at around 3 GPa, i.e. at 100 km depth. This corresponds with a depth of the spinel-garnet transitional field (Robinson and Wood, 1998; Klemme and O'Neill, 2000; Klemme, 2004). At such depth, dry peridotite could not melt up to a mantle potential temperature of 1450^{o}C, therefore presence of water or pyroxenite/eclogite with lower solidus is expected in the source region that may lead to lower the calculated pressure (Wang et al., 2002). Nevertheless, the final depth of melting columns of the CPR basalts is between 2.1 and 2.5 GPa (70-83 km depth), what is in good agreement with the geophysically determined thickness of the lithosphere (Horváth et al., 2006) beneath the volcanic fields (Fig. 7). In addition to the usual melting depth of the CPR basalts, the alkaline basalts from Burgenland (Pauliberg and Oberpullendorf) fall into the 3.4 and 3.8 GPa melting lines (Fig. 6A) that corresponds with an onset of melting at greater depth (110-125 km). This fits, however, well with the deep structure beneath these basaltic volcanoes, i.e. they are located in an area characterized by thick lithosphere (ca. 110 km present day thickness; Fig. 7). The relatively shallow melting column beneath the Perşani volcanic field (86-70 km depth interval) seems to be remarkable, since formerly Dérerova et al. (2006) and Horváth et al. (2006) suggested a thick lithosphere here (about 140 km). However, Harangi et al. (2013) pointed out that the Perşani basaltic magmas were originated by melting of asthenospheric mantle and therefore the LAB should be much shallower, i.e. not deeper than 60 km. This is consistent with the geophysical result of Martin et al. (2006) and implies that a narrow rupture could have developed in the lower lithosphere beneath the Perşani area, probably as a result of the dragging effect of the descending dense lithospheric slab beneath the Vrancea zone located about 100 km from the volcanic field (Harangi et al., 2013). In two cases (Putikov vŕšok and Lucaret), we got a melting column fairly deep in comparison with the lithospheric thickness. Partial melting could start here deeper than 100

548 km and terminated shortly after 10-15 km mantle upwelling. A possible explanation for this
549 would be the exhaustion of the fusible material such as hydrous peridotite or garnet-
550 pyroxenite/eclogite.
551 An independent test of the result provided by the Langmuir et al. (1992) model can be
552 achieved with comparison of the primary magma compositions of the CPR basalts with
553 experimental data sets (Sakuyama et al., 2009) and using other geobarometric calculations
554 (Scarrow and Cox, 1995; Lee et al., 2009). Sakuyama et al. (2009) compiled results of various
555 melting experiments and suggested that SiO_2 content of the primary melt is the most sensitive
556 parameter on melting pressure in the range of 1.0-3.0 GPa and it does not depend significantly
557 on the degree of melting, the initial bulk composition and modal mineralogy. Water content of
558 the source peridotite could slightly increase the SiO_2 content of the melt at constant pressure
559 (Hirose and Kawanoto, 1995) that may lead to slight underestimation of the pressure if dry
560 peridotite melting is considered. Plotting the primary magma compositions of the CPR basalts
561 on the ol'-ne'-qtz' triangular diagram along with the isobaric melting lines as determined by
562 Sakuyama et al. (2009) based on experimental data sets, 2.5-3.5 GPa melting pressures are
563 obtained (Fig. 6B) that are in good agreement with the constrains on the melting columns
564 described above, particularly with the initial melting pressure. The only exception is the
565 basalts from Lucaret for which we got melting pressure of 2.5 GPa, significantly lower than
566 from the Langmuir et al. (1992) model (3.20-2.75 GPa). Scarrow and Cox (1995) developed a
567 simple equation for the melting pressure estimate based on the SiO_2 content of primary rocks.
568 It gives slightly lower pressure values than the ol'-ne'-qtz' diagram, whereas the corrected
569 SiO_2-geobaromether by Wang et al. (2002) appears to strongly overestimate the pressure
570 particularly at higher pressure (>2.5 GPa). Finally, we applied also the peridotite-melt
571 barometer of Lee et al. (2009), which gives consistent result with the SiO_2-barometer of
572 Scarrow and Cox (1995), but also with the final pressure estimate of the Langmuir et al.

573 (1992) model (Fig. 8). There is also a good correlation between the pressure obtained by the
574 Lee et al. (2009) barometry and the qtz'/(ol'-ne'-qtz') ratio, which was suggested as a
575 sensitive parameter of depth of melting (Sakuyama et al., 2009). The only exception is the
576 basalts from Pauliberg that form a parallel trend at slightly higher pressure range, probably
577 due to the difference of the source lithology.

578 In summary, we can conclude that melting of the upwelling asthenospheric mantle
579 material could start at about 100 km depth beneath most of the volcanic fields of the CPR and
580 the final melting pressure could have been controlled by the thickness of the lithosphere, i.e.
581 the lithosphere-asthenosphere boundary. Partial melting occurred at greater depth beneath
582 Pauliberg, which is underlain by thicker lithosphere, whereas beneath the Perşani area melting
583 could have taken place at shallower depth due to a local rupture of the lower lithosphere. The
584 youngest basalt beneath Putikov vŕšok generated at greater depth (100-120 km), whereas the
585 2.4 Ma Lucaret basalt could have been derived also from a relatively shallow depth in spite of
586 the higher FeO content of the basalts.

587

588 ***Conditions of melt generation***

589

590 We proposed that partial melting of the upwelling asthenospheric mantle material
591 could lead to the generation of basaltic magmas, which fed the volcanic eruptions in the
592 monogenetic volcanic fields of the CPR. A further constrain on the melt generation process
593 can be obtained from trace element petrogenetic modelling (Fig. 9). We used different initial
594 compositions (depleted MORB mantle and slightly enriched primitive mantle; Salters and
595 Stracke, 2004; McDonough and Sun, 1995) and different mineralogical assemblage (garnet-
596 lherzolite, spinel lherzolite) of the source material and different melting models (batch and
597 fractional melting; Shaw, 1970; critical or dynamic melting; Sobolev and Shimizu, 1992; Zou,

1998; Shaw, 2000) with the mineral-melt distribution coefficients proposed by Kostopoulos and James (1992). Trace element ratios of Zr/Nb and La/Y were chosen, because their values are not dependant on early-stage crystal fractionation and are sensitive (La/Y) on the presence of spinel and garnet in the mantle source. As we discussed earlier, it is unlikely that amphibole was also present in the source region of the CPR basalts and therefore, it was not considered in the modelling calculations. The result of the petrogenetic modelling is shown in Figure 9.

The primary magmas of the CPR basalts were formed from trace element enriched mantle source (1.5-4.0-times of the primitive mantle composition; McDonough and Sun, 1995) within the spinel-garnet transitional zone (Fig. 9.). The degree of melting is somewhat model dependant, but it is between 1.5% and 5%. The best fit of the CPR basalts with the melting model lines is given assuming continuous dynamic melting or decompressional critical melting (Sobolev and Shimizu, 1992; Zou, 1998; Shaw, 2000) process. This model is consistent with the melting process described in the previous section, i.e. commencing of melting in a mantle source, where garnet prevails over spinel and then continues in the spinel stability field. In this case, 2-3% melting is required to obtain the composition of the primary basaltic magmas of the CPR. Noteworthy, the Lucaret basalts fall on the spinel-peridotite melting line implying shallow melting and suggest that the FeO content of the bulk rock overestimates the melting pressure and the SiO_2-based geobarometries provide more reliable result. On the other hand, the basalts from the western Pannonian Basin (Pauliberg, Oberpullendorf and Klöch from the Styrian basin) fall on the garnet-peridotite melting line consistent with their derivation from a deeper source.

The depth of melting for the CPR basalts as shown by various models is between 60 and 120 km. The associating melting temperature can be determined using the peridotite-melt thermometer by Lee et al. (2009; using molar Fe^{3+}/Fe^{tot}=0.13) and the PRIMELT2 software of

623 Herzberg and Asimow (2008; using Fe_2O_3=TiO_2). They resulted in fairly similar temperature
624 values up to 1470^{o}C (Fig. 7), where the Lee et al. (2009) calculation tends to give much
625 higher (>100^{o}C) temperature than the PRIMELT2 (mostly for the Pauliberg basalts). The
626 lowest mantle potential temperature is shown by the Perşani basalts (1310-1380^{o}C) that
627 records indeed shallow melting as indicated by the geobarometric calculations, whereas in the
628 other volcanic fields, we got melting temperature in a range between 1350 and 1450^{o}C. The
629 highest potential temperature values were obtained for the basalts at Pauliberg (>1440^{o}C) and
630 at Putikov vŕšok (1420-1450^{o}C).
631 Taken together the obtained pressure and temperature values, the Figure 10 shows that
632 the melting columns of the basaltic magmas of the CPR are just below the dry peridotite
633 solidus. This requires either some water or a more fusible material, such as pyroxenite or
634 eclogite in the mantle source. The relatively low CaO content (<10 wt%) of the calculated
635 primary basaltic magmas as well as the low Ca also in the olivine phenocrysts (Harangi et al.,
636 2013) are features that can be explained by pyroxenite melting (Herzberg, 2011). However,
637 the olivine in the CPR basalts (Embey-Isztin and Dobosi, 2007; Jankovics et al., 2012; 2013;
638 Harangi et al., 2013) has relatively low Ni and high Mn concentrations that is just the opposite
639 of what required in the case of pyroxenite melting (Sobolev et al., 2007). These features could
640 be explained, however, also by the lid-effect, i.e. by variations in lithospheric thickness (Niu
641 et al., 2011). Magmas generated under a thin lithosphere could crystallize olivines with
642 relatively low Ni and high Mn and corresponding low Ni/Mg, low Ni/(Mg/Fe) and high
643 Mn/Fe and high Ca/Fe ratios. Although the Ca deficiency of the olivine and the host rocks of
644 the CPR is still unresolved, it appears that the basaltic magmas beneath the CPR could have
645 originated dominantly from a peridotitic mantle source. In this case, however, some water
646 (50-200 ppm; Hirschmann et al., 2009) should be present in the source region. The origin of
647 this volatile content can be explained either by the supposed intense Palaeogene-Miocene

subduction around the Carpathians (Csontos et al., 1992) or dewatering of the accumulated subducted material in the transitional zone (Hetényi et al., 2009). An important point coming from the Figure 10. is that the upper mantle beneath the thin continental lithosphere of the Pannonian basin has a temperature close to the peridotite solidus and the mantle could be partially hydrous that makes it potentially still fusible. Eruptions of basaltic magmas in the last 2 Ma could confirm the potentially fusible state of the mantle. The low seismic velocity anomaly down to the transitional zone beneath the northern part of the Pannonian basin (Dando et al., 2011) could provide a further supporting evidence of this.

Mantle source characteristics

Chromian spinels enclosed by olivine phenocrysts could provide important information about the mantle sources of the CPR basalts. They occur in each volcanic field and therefore it can be used to gain insights into the nature of the sublithospheric mantle on a regional scale. Chromian spinel is often the liquidus phase along with olivine in basaltic melts (Fisk and Bence, 1980; Luhr and Carmichael, 1985), therefore it reflects the primary characteristics of the basaltic melt. It can be used for deciphering the original magmatic characteristics even of heavily altered basalts (Allan, 1992). Composition of the liquidus spinels is considered to be close to that of the spinels in the residual mantle source region, although other controlling factors such as magma differentiation, crystallization pressure, redox condition and the degree of partial melting also influence the composition of spinels (Hill and Roeder, 1974; Sigurdsson and Schilling, 1976; Dick and Bullen, 1984; Allan et al., 1988; Roeder and Reynolds, 1991; Arai, 1994; Clynne and Borg, 1997; Kamenetsky et al., 2001; Roeder et al., 2003).

672 The spinel inclusions found in the CPR basalts show a wide compositional range (cr-
673 number=0.15-0.68, mg-number=0.2-0.8). They are mostly chromian spinels thought to be
674 formed as early-stage mineral phases, however, as soon as they became out of the narrow
675 temperature interval where they could appear as liquidus crystals (Sigurdsson and Schilling,
676 1976; Fisk and Bence, 1980; Luhr and Carmichael, 1985), they react with the differentiated
677 melt and the spinel component is rapidly replaced by magnetite and ulvöspinel components
678 increasing their FeO and Fe_2O_3, and TiO_2 contents (Luhr and Carmichael, 1985; Clynne and
679 Borg, 1997; Arai, 1992; Roeder et al., 2003). Therefore, we selected spinels enclosed by the
680 most magnesian (Fo>84 mol%) olivines and then, we filtered out the analyzed spinel
681 compositions using their TiO_2 and Fe^{3+}-number in order to focus on the most primitive spinel
682 population. Instead of using a definite limit of these parameters (e.g., Clynne and Borg, 1987),
683 we plot all the data on the Cr-Fe^{3+}-Al triangular diagram and compared them with the natural
684 basalt-hosted spinel compositional range (Barnes and Roeder, 2001). The majority of the
685 MORB spinels show a wide variation in the Cr-Al trend, whereas many spinels from OIB
686 have a slight enrichment in Ti and Fe. We selected the spinel population thought to represent
687 liquidus mineral phases primarily based on the overlap with the 50^{th} percentiles of the OIB
688 and MORB spinels and then we considered the possible differentiation trends. The whole data
689 set and the selected "liquidus-spinel" compositions are shown in Fig. 11. The primary spinels
690 form four coherent groups in the Cr-Fe^{3+}-Al diagram that could represent different mantle
691 domains beneath the CPR. Three of them appear in all major volcanic fields of the CPR,
692 whereas the forth one belongs solely to the Pauliberg location. In general, spinel composition
693 closely mimics the host rock composition (as shown by the correlation between the cr-number
694 of spinels and the $Fe_2O_3^t$, Al_2O_3 and TiO_2 contents of the host rock). The basanites of
695 Pauliberg have a specific composition within the Miocene-Quaternary alkaline basalts of the
696 CPR (Embey-Isztin and Dobosi, 1995; Ali and Ntaflos, 2011) showing depletion in Al and

enrichment in Fe and Ti compared with the others. Spinels in these rocks are also depleted in Al (thus, they have relatively high cr-number) and slightly enriched in Fe and Ti, plotting outside from the MORB and OIB spinel fields. Nevertheless, considering the specific composition of their host rock, they could also belong to the "liquidus-spinel" population and reflect a particular mantle source region of the Pauliberg magmas. Tentatively, this might be a sign of involvement of eclogite during melting, a hypothesis that requires further studies.

Compositional characters of the spinels are controlled by many factors as listed before. Influence of the magma differentiation could be filtered out by limiting the data set to the most primitive spinels. The pressure of crystallization affects predominantly the Al content of the chromian spinels (Dick and Bullen, 1984) showing positive correlation between them. The large compositional variation of the spinel compositions in the CPR basalts, however, could be unlikely related to the variable crystallization pressures, since the lowest Al content in spinels was recorded in those basalts which were interpreted as derived from the deepest source (Pauliberg, Putikov, Lucaret). Spinel composition is dependant also on the degree of partial melting as demonstrated by Arai (1994) and Baker and Stolper (1994). The cr-number of spinel in the mantle restite rock increases with increasing degree of melting. Spinels with 0.10-0.15 cr-number are considered to represent fertile mantle regions, whereas spinels with cr-number of about 0.6 could indicate more than 25% degree of melting (Baker and Stolper 1994). However, no correlation can be recognized between the variation of spinel cr-number and the incompatible trace element ratios of the CPR basalts that are sensitive on the progressive melting process (e.g., La/Y, $[Sm/Yb]_N$). Furthermore, our petrogenetic model calculation suggests that the mafic magmas of CPR could have originated by 2-3% of melting and therefore, the large compositional variation of spinels cannot be attributed to various degrees os partial melting. Taking all of these into account, we can conclude that the spinels in the CPR basalts reflect the nature of the mantle source region, more precisely the character

of the residual mantle rocks and indicates heterogeneous, variably depleted sublithospheric mantle beneath the Pannonian basin.

Spinel compositions suggest that at least three main compositional domains (and a specific one beneath Pauliberg) could exist in the mantle source region and they are well distributed beneath each volcanic field. Although the composition of the liquidus spinels is close to the spinels in the restitic mantle rocks rather than in the intitial source material, the small degree of melting characterizing the CPR basalts could not significantly modify the compositional feature of the intial spinels as also emphasized by Clynne and Borg (1997) for the Lassen basalts. Therefore, the composition of the restite spinels could be close to that of the initial ones. Noteworthy, the youngest (<600 ka) basalts could have derived either from the most fertile mantle source domain (Perşani basalts; spinel cr-number=0.23-0.32; Harangi et al., 2013) or from a mantle domain akin to enriched OIB (Putikov vŕšok; spinel cr-number=0.55-0.61; TiO_2=2.0-3.5 wt%; Ságiet al., in prep). This might mean that the sublithospheric mantle beneath CPR could be potentially still capable to produce basaltic magmas, i.e. contains fusible parts of material.

Geodynamic relationships

The origin of the alkaline basaltic volcanism in the CPR seems to be enigmatic since it occurred after the main phase of the lithospheric extension of the Pannonian basin (20-15 Ma; Horváth et al., 2006), during the stage of post-rift thermal subsidence and tectonic inversion. Melt generation has taken place intermittently since 11 Ma with a peak period between 5 and 1 Ma. In such situations, hot mantle upwelling beneath the thinned lithospheric realm seems to be a viable mechanism to produce low-volume basaltic magma (Embey-Isztin et al., 2001; Harangi, 2001b). Composition of the Neogene alkaline mafic rocks in Europe shares many

747 similarities, particularly in the radiogenic isotope ratios. Taking this into account and
748 correlating it with seismic anomalies in the sublithospheric mantle beneath Europe, Hoernle et
749 al. (1995) and Granet et al. (1995) proposed a common mantle reservoir of the mafic magmas
750 (called European Asthenospheric Reservoir; EAR by Cebriá and Wilson, 1995) that fed the
751 basaltic volcanism via localized active mantle plumes ("plume finger") in different parts of
752 Europe, such as in the Massif Central, the Rhenish area, the Eger graben, Bohemia and also in
753 the Pannonian basin (Granet et al., 1995; Wilson and Patterson, 2001). The plume finger
754 model was put forward for the Pannonian basin by Embey-Isztin et al. (2001), Seghedi et al.
755 (2004b) and Seghedi and Downes (2011). Seghedi et al. (2004b) distinshuished at least three
756 plume fingers beneath the CPR, primarily based on the HIMU-like isotopic character of the
757 basalts. However, we have to emphasize that the HIMU-like isotopic ratios have solely a
758 descriptive message and this does not necessarily mean plume-origin. Nevertheless, the
759 plume-related basaltic magmatism in the CPR was proposed also by other authors based on
760 geological, geochemical and geophysical considerations (Goes et al., 1999; Buikin et al.,
761 2005; Burov and Cloetingh, 2009). In contrast, Harangi and Lenkey (2007) argued against a
762 mantle plume beneath the Pannonian basin.
763 There are a couple of observations that are not consistent with the plume model.
764 Beneath the Pannonian basin, in the depth range of 400-650 km, a positive seismic velocity
765 anomaly is recognized (Wortel and Spakman, 2000; Piromallo et al., 2001; Piromallo and
766 Morelli, 2003; Hetényi et al. 2009). The origin of this anomaly was postulated as
767 accumulation of thick, cold material, possibly subducted residual material supplied from
768 several subduction episodes (Penninic in the Cretaceous, Vardar in the Palaeogene, and the
769 East Carpathian subduction in the Miocene; Hetényi et al. 2009). This vast amount of cold
770 material can form a barrier against the rise of any lower mantle-derived plume and prevents
771 the initiation of upwelling of hot material from the Transition Zone. However, it has been

772 shown that the Transitional Zone could be one of the wettest parts of the upper mantle,
773 particularly when subducted material is accumulated there for a long time (Hirschmann, 2006;
774 Karato, 2011). Thus, it could serve as the source for wet plumes instead of hot plumes. In this
775 scenario, wet melting in the upper part of the Transition Zone (Hirschmann, 2006) could
776 provide small volume hydrous magmas that initiate further melting beneath the continental
777 lithosphere. Although this is a reasonable scenario it does not explain the observation why the
778 basaltic volcanic fields are at the marginal parts of the Pannonian basin and not in the central
779 areas. The characteristic features of hot mantle plumes are also missing in the CPR. The broad
780 topographic updoming such as detected in the Massif Central (Wilson and Patterson, 2001), or
781 in classic hot spot areas (Courtillot et al., 2003), is absent; on the contrary, some parts of the
782 Pannonian Basin are still subsiding. The high heat flow in the CPR (Lenkey et al., 2002) can
783 be readily explained by the thinning of the lithosphere during basin formation and by the still
784 shallow asthenosphere (Royden et al., 1982). As far as the HIMU-like isotopic ratios of some
785 CPR basalts are concerned, they could have also a metasomatic origin (e.g., Hart, 1988; Sun
786 and McDonough, 1989; Halliday et al., 1995; Pilet et al., 2005). The sporadic distribution and
787 the low-magma output type of the volcanic fields in the CPR also do not support any hot
788 mantle plume origin. Therefore, there are no supporting evidences that favour hot mantle
789 plume or plume finger (Seghedi et al., 2004) origin of the basaltic volcanism in the CPR.
790 Generation of basaltic magmas in the asthenosphere requires upward movement of
791 solid mantle material, i.e. a mantle flow. In this context, the spatial distribution of the basalt
792 volcanic fields at the peripheral areas of the CPR could have relevance. They occur above a
793 lithosphere-asthenosphere boundary with sharp depth variation between the orogenic Alps
794 and cratonic North European Platform with thick (>160 km) lithospheric roots and the
795 stretched Pannonian basin with thin (< 70 km) lithosphere within relatively short distances
796 (Fig. 12.). The Pannonian basin could therefore act as a thin-spot providing suction in the

797 sublithospheric mantle and generating mantle flow from below the thick lithospheric roots
798 (Harangi and Lenkey, 2007; Harangi, 2009). The SKS splitting measurements show a
799 dominant west-east direction beneath the western part of the Pannonian basin with a clear
800 continuation from the Alps and this direction changes to a northwest-southeast trend toward
801 the central and northern areas (Kovács et al. 2012). On the western side of the Alps, similar,
802 east-west directed SKS splitting directions were recognized that turn gradually in north-south
803 direction northward and this was considered as relatively recent asthenospheric flow (Barroul
804 et al. 2011). Remarkably, a similar seismic pattern was observed also in the Lake Baikal area,
805 where it was interpreted as sublithospheric mantle flow from beneath the thick Siberian craton
806 towards the thin Baikal–Mongolian area (Lebedev et al., 2006). The low-volume, scattered,
807 and sporadic basalt volcanism in the Baikal rift could have been connected with this mantle
808 flow by decompression melting when the asthenospheric material ascended from the 200-km
809 depth beneath the craton to shallower depths beneath the rift (Lebedev et al., 2006). A similar
810 triggering mechanism was put forward by Niu (2005) explaining the basaltic volcanism in the
811 East China lowland. Thus, it appears that a large contrast in the LAB architecture could
812 enhance mantle flow that results in intraplate basaltic volcanism with many similarities to
813 OIB-type compositions. This appears to be the case also in the Alps-Pannonian basin
814 transition zone, where relatively hot asthenospheric material could ascend from beneath the
815 Alps along the steep LAB (Harangi, 2009; Fig. 13). The important role of asthenospheric
816 mantle flow as a driving force for the Neogene extension and extrusion events is getting to
817 have an increasing attention in the geodynamic model of the Pannonian basin. Konečný et al.
818 (2002) invoked an asthenospheric flow due to subduction roll-back mechanism and explained
819 the magma generation by this process. Kovács et al. (2012) proposed that this mantle flow is
820 the result of the convergence between the Eurasian and African plates along the Alpine belt,
821 whereas Horváth and Faccenna (2011) suggested that mantle material was pumped through

822 the Istria slab window beneath the CPR mantle as a result of slab rollback along the eastern
823 margin of the region. An important difference between these models and the explanation put
824 forward in this paper is the time of the mantle flow. According to Konečný et al. (2002),
825 Kovács et al. (2012) and Horváth and Faccenna (2011) this process could have been taking
826 place since the Oligocene/Miocene and act as a major role in the geodynamic evolution of the
827 CPR, whereas here, we propose that it is a passive process commenced just after the Mid-
828 Miocene formation of the Pannonian basin with strongly thinned lithosphere and in this case
829 this thin spot condition acted as a driving force of the mantle flow.
830 In the northern part of the Pannonian basin, there has been a long lasting volcanic
831 activity since about 16 Ma (Harangi et al., 2007). The alkaline basalt volcanism followed an
832 intense calc-alkaline volcanic period (Konečný et al., 1995; 2002). Nevertheless, no traces of
833 subduction-related mantle source are observed in the composition of the basaltic products. It
834 can be explained by effective change in the sublithospheric mantle beneath the Štiavnica and
835 Nógrád-Gemer area that could require again mantle flow mechanism. In the seismic
836 tomography model sections published by Dando et al. (2011) a low-velocity anomaly can be
837 observed beneath this region that has a continuation into the deeper mantle towards north.
838 Tentatively, this can be interpreted as a sign of an upward flow beneath the steep LAB. The
839 low magma output and the sporadic eruption events over several million years long period (8-
840 0.1 Ma) could suggest, however, a tectonic control of the melt generation-magma ascent
841 processes. Strain localization in the upper mantle beneath major faults that penetrate the upper
842 mantle (Leloup et al. 1995; Vauchez et al., 2012) could be a possible mechanism of this.
843 Reactivation of transtensional tectonic lines could have a close link with the tectonic inversion
844 of the Pannonian basin (Horváth and Cloetingh, 1996) that started in the Late Miocene when
845 the peak magma-output phase occurred in the Bakony-Balaton Upland and the Štiavnica and

Nógrád-Gemer volcanic fields. Further research could focus on the interrelationship of tectonic processes along pre-existing lines and the volcanic events.

The youngest basalt volcanic field was developed at the eastern part of the CPR (Perşani area; Seghedi and Szakács, 1994; Downes et al., 1995) from 1.2 to 0.6 Ma (Panaiotu et al., 2013). Seghedi et al. (2011) invoked toroidal asthenospheric flow around the downgoing slab beneath Vrancea to explain the localized alkali basalt volcanism, whereas Harangi et al. (2013) proposed that this could have occurred as a response to the formation of a narrow rupture in the lower lithosphere, possibly as a far-field effect of the dipping of dense continental lithospheric material beneath the Vrancea zone. Upper crustal extensional stress field with reactivation of normal faults at the eastern margin of the Transylvanian basin could enhance the rapid ascent of the mafic magmas.

Finally, it is remarkable that local low-velocity mantle anomaly has been detected beneath both the Štiavnica and the Perşani areas (Dando et al., 2011; Popa et al., 2012) that along with our interpretation about the presence of mantle region containing still fusible material suggest that further volcanic eruptions cannot be unambiguously excluded in these areas. The rapid ascent of the magmas (Harangi et al., 2013; Jankovics et al., 2013) implies that the quiet situation could change rapidly.

Summary

Evaluation of the major and trace element content of the most primitive basalts in the CPR along with the interpretation of the most primitive spinel compositions indicates that the primary magmas could have generated in the convective asthenosphere. Trace element modelling indicates incompatible trace element-enriched source composition and 2-3% melting within the garnet-spinel transition zone. Melting started at about 100 km depth where

garnet prevails over spinel and continued usually up to the base of the lithosphere. Thus, the final melting pressure could indicate the ambient lithosphere-asthenosphere boundary (LAB). The asthenospheric mantle source regions of the basalts were heterogeneous, presumably at small scale. Spinel compositions show a wide range, although four coherent groups can be distinguished that are interpreted as reflect the main mantle domains beneath this region. They can be recognized at almost each volcanic field. Two of these have fertile and slightly depleted character, respectively, whereas the two others are enriched in Fe and Ti and overlap the spinels found in the basalts of Hawaii. They might indicate involvement of pyroxenitic/eclogitic lithology in the melting process that requires further investigation. Major element composition of some of the basalts (low Al and high Ti and Fe; e.g., Pauliberg, Putikov) could be also consistent with melting of carbonated, silica-deficient eclogite. Indeed, considering the depths of the estimated melting columns of the CPR basaltic magmas, a more fusible material than the dry peridotite is required in the source regions of the magmas. Presence of water or pyroxenite/eclogite could explain melting at such depth.

The prevailing estimated mantle potential temperature (1300-1400^{o}C) along with number of further observations do not require anomalously hot asthenospheric mantle. Thus, we can exclude the presence of any mantle plume or mantle plume fingers beneath the Pannonian basin. The locations of the monogenetic basalt volcanic fields at the western and northern margin of the Pannonian basin could indicate a close relationship with the steep LAB beneath these areas. We propose that asthenospheric flow from beneath the adjoining thick lithospheric domains (Alps, cratonic North European Platform) to the thinned Pannonian basin could play a triggering role in the melt generation. A near vertical upwelling along the steep LAB could result in decompressional melting producing low-volume melts. The Pannonian basin could therefore act as a thin-spot after the Mid-Miocene syn-rift phase (20-12 Ma) and provided suction in the sublithospheric mantle generating asthenospheric flow

from below the thick lithospheric roots. In addition to this dominant process, single basaltic volcanic events in the inner part of the Pannonian basin could have been related to strain-localization in the upper mantle beneath major strike-slip faults that penetrate the upper mantle. Further southeast, close to the Vrancea zone, the youngest basalt volcanic field in the CPR could have been formed as a plate tectonic response of the dipping dense continental lithospheric material. The suction of the descending lithospheric slab could result in narrow rupture at the base of the lithosphere. Decompression melting of the upwelling asthenospheric mantle could result in magma generation, while reactivation of normal faults enhanced the rapid ascent of the magmas.

Origin of basaltic magmas with fairly primitive composition for the last 1 Ma implies that fusible material could still exists in the mantle, which have a potential temperature close to the solidus. This inferred condition and the low-velocity anomalies detected in the mantle depths as well as the still high localized heat flows in these areas all suggest that continuation of the basaltic volcanism in the CPR cannot be unambiguously excluded.

Acknowledgement

Our ideas about the basaltic volcanism in the Carpathian-Pannonian region have refined during number of instructive and sometimes heavy discussions with several colleagues such as Hilary Downes, Theodoros Ntaflos, Ioan Seghedi, Frank Horváth, Károly Németh, Csaba Szabó, István Kovács, Orlando Vaselli, László Lenkey, Marge Wilson, Michele Lustrino, Jaroslav Lexa, Kadosa Balogh, Zoltán Pécskay and László Fodor. These were promoted by great workshops started with the PANCARDI meetings in the 1990's and early 2000's, followed by the ILP PLUME workshop at Mt. Sainte-Odile in 2006, the EMAW conference in Ferrara, 2007 and the Basalt2013 in Görlitz in 2013. Discussions about the

mantle potential temperature calculations with Claude Herzberg and Keith Putirka were particularly stimulated. Terry Plank kindly provided the calculation scheme of the Langmuir et al. (1992) melting model. Participation of the young scientists, M. Éva Jankovics, Balázs Kiss and Réka Lukács was supported in this research by the European Union and the State of Hungary, co-financed by the European Social Fund in the framework of TÁMOP-4.2.4.A/2-11/1-2012-0001 `National Excellence Program'. Constructive comments provided by Stefan Jung and an anonymous reviewer helped us to clarify our views.

References

Aldanmaz E, Koprubasi N, Gurer ÖF, Kaymakci N, Gourgaud A (2006) Geochemical constraints on the Cenozoic, OIB-type alkaline volcanic rocks of NW Turkey: Implications for mantle sources and melting processes. Lithos 86:50-76.

Ali S, Ntaflos T (2011) Alkali basalts from Burgenland, Austria: Petrological constraints on the origin of the westernmost magmatism in the Carpathian-Pannonian Region. Lithos, 121:176-188

Ali S, Ntaflos T, Upton BGJ (2013) Petrogenesis and mantle source characteristics of Quaternary alkaline mafic lavas in the western Carpathian-Pannonian Region, Styria, Austria. Chemical Geology, 337-338:99-113.

Allan JF (1992) Cr-spinel as a petrogenetic indicator: deducing magma composition from spinel in highly altered basalts from the Japan Sea, Sites 794 and 797. Proc. Ocean Drilling Program 127/128:837-847.

Allan JF, Sack RO, Batiza R (1988) Cr-rich spinels as petrogenetic indicators; MORB-type lavas from the Lamont seamount chain, eastern Pacific. American Mineralogist 73:741-753.

946 Arai S (1992) Chemistry of chromian spinel in volcanic rocks as a potential guide to magma
947 chemistry. Mineralogical Magazine 56:173-184.
948 Arai S (1994) Compositional variation of olivine-chromian spinel in Mg-rich magmas as a
949 guide to their residual spinel peridotites. Journal of Volcanology and Geothermal
950 Research, 59:279-293.
951 Bada G, Horváth F, Fejes I, Gerner P (1999) Review of the present-day geodynamics of the
952 Pannonian basin: progress and problems. Journal of Geodynamics, 27:501–527.
953 Baker MB, Stolper EM (1994) Determining the composition of high-pressure mantle melts
954 using diamond aggregates. Geochim. Cosmochim. Acta 58:2811-2827.
955 Balázs E, Nusszer A (1987) Unterpannonischer Vulkanismus der Beckengebiete Ungarns.
956 Annales of Hungarian Geological Institute, 69:95-104.
957 Balogh K, Németh K (2005) Evidence for the Neogene small-volume intracontinental
958 volcanism in the Western Hungary: K/Ar geochronology of the Tihany Maar Volcanic
959 Complex. Geologica Carpathica 56:91–99.
960 Balogh K, Mihalikova A, Vass D (1981) Radiometric dating of basalt in Southern and Central
961 Slovakia. Zap. Karpaty, ser. Geol. 7:113 126.
962 Balogh K, Jámbor A, Partényi Z, Ravaszné Baranyai L, Solti G (1982) A dunántúli bazaltok
963 K/Ar radiometrikus kora. A Magyar Állami Földtani Intézet Évi Jelentése az 1980.
964 évről:243-259.
965 Balogh K, Árva-Sós E, Pécskay Z, Ravasz-Baranyai L, (1986) K/Ar dating of post-Sarmatian
966 alkali basaltic rocks in Hungary. Acta Mineralogica et Petrographica Szeged 28:75-93.
967 Balogh K, Harald L, Pécskay Z, Ravasz Cs, Solti G (1990) K/Ar radiometric dating of the
968 Tertiary volcanic rocks of East-Styria and Burgenland. MÁFI Évi Jel. 1988-ról:451-
969 468.

970 Balogh K, Ebner F, Ravasz Cs (1994) K/Ar alter tertiärer Vulcanite de südöstlischen
971 Steiermark und des südlischen Burgenlands. In: Császár, G, Daurer, A. (Eds.),
972 Jubiläumsschrift 20 Jahre Geologischen Zusammenarbeit Österreich-Ungarn Lobitzer,
973 55–72.
974 Balogh K, Itaya T, Németh K, Martin U, Wijbrans J, Thanh NX (2005) Study of controversial
975 K/Ar and 40Ar/39Ar ages of the Pliocene alkali basalt of Hegyestű, Balaton Highland,
976 Hungary: a progress report. Mineralia Slovaca 37:298–300.
977 Barnes SJ, Roeder PL (2001) The Range of Spinel Compositions in Terrestrial Mafic and
978 Ultramafic Rocks. Journal of Petrology 42:2279-2302.
979 Barruol G, Bonnin M, Pedersen H, Bokelmann GHR, Tiberi C (2011) Belt-parallel mantle
980 flow beneath a halted continental collision: the Western Alps. Earth and Planetary
981 Science Letters, 302:429-438
982 Beccaluva L, Bianchini G, Bonadiman C, Coltorti M, Milani L, Salvini L, Siena F, Tassinari
983 R (2007) Intraplate lithospheric and sub-lithospheric components in the Adriatic
984 domain: Nephelinite to tholeiite magma generation in the Paleogene Veneto Volcanic
985 Province, Southern Alps. In: Beccaluva, L, Bianchini, G, Wilson, M. (Eds.), Cenozoic
986 Volcanism in the Mediterranean Area: Geological Society of America, Special paper,
987 418:131–152.
988 Beccaluva L, Bianchini G, Natali C, Siena F (2011) Geodynamic control on orogenic and
989 anorogenic magmatic phases in Sardinia and Southern Spain: Inferences for the
990 Cenozoic evolution of the western Mediterranean. Lithos, 123:218–224.
991 Bianchini G, Beccaluva L, Siena F (2008) Postcollisional and intraplate Cenozoic volcanism
992 in the rifted Apennines/Adriatic domain. Lithos, 101:125–140.

993 Blondes MS, Reiners PW, Ducea MN, Singer BS, Chesley J (2008) Temporal-compositional
994 trends over short and long time-scales in basalts of the Big Pine Volcanic Field,
995 California. Earth and Planetary Science Letters 269:140-154.
996 Borsy Z, Balogh K, Kozák M, Pécskay Z (1986) Újabb adatok a Tapolcai-medence
997 fejlõdéstörténetéhez. Acta Geographica Debrecina 23:79-104.
998 Bradshaw, TK, Hawkesworth CJ, Gallagher K (1993) Basaltic volcanism in the Southern
999 Basin and Range: no role for a mantle plume. Earth and Planetary Science Letters,
1000 116:45-62.
1001 Brenna M, Cronin SJ, Smith IEM, Sohn YK, Németh K (2010) Mechanisms driving
1002 polymagmatic activity at a monogenetic volcano, Udo, Jeju Island, South Korea.
1003 Contributions to Mineralogy and Petrology 160:931-950.
1004 Brenna M, Cronin SJ, Smith IEM, Maas R, Sohn YK (2012) How small-volume basaltic
1005 magmatic systems develop: a case study from the Jeju Island Volcanic Field, Korea.
1006 Journal of Petrology 53:985-1018.
1007 Buikin A, Trieloff M, Hopp J, Althaus T, Korochantseva E, Schwarz WH, Altherr R (2005)
1008 Noble gas isotopes suggest deep mantle plume source of late Cenozoic mafic alkaline
1009 volcanism in Europe. Earth and Planetary Science Letters, 230:143-162.
1010 Burov E, Cloetingh S (2009) Controls of mantle plumes and lithospheric folding on modes of
1011 intraplate continental tectonics: differences and similarities. Geophysical Journal
1012 International, 178:1691-1722.
1013 Cebriá, JM, Wilson M (1995) Cenozoic mafic magmatism in western/central Europe: A
1014 common European asthenospheric reservoir? Terra Nova, 7:162.
1015 Cebriá JM, López-Ruiz J (1995) Alkali basalts and leucitites in an extensional intracontinental
1016 plate setting: The late Cenozoic Calatrava Volcanic Province (central Spain). Lithos,
1017 35:27-46.

1018 Chaffey DJ, Cliff RA, Wilson BM (1989) Characterization of the St. Helena magma source. –
1019 In: Saunders AD, Norry MJ (Eds) Magmatism in the Ocean Basins. Geological
1020 Society Special Publication, 42:257-276.
1021 Chernyshev IV, Konečný V, Lexa J, Kovalenker VA, Jeleň S, Lebedev VA, Goltsman YV
1022 (2013) K-Ar and Rb-Sr geochronology and evolution of the Štiavnica Stratovolcano
1023 (Central Slovakia). Geologica Carpathica 64: 327-351
1024 Class C, Goldstein SL (1997) Plume–lithosphere interactions in the ocean basins: constraints
1025 from the source mineralogy. Earth and Planetary Science Letters 150:245–260.
1026 Cloetingh SAPL, Ziegler PA, Bogaard PJF, Andriessen PAM, Artemieva IM, Bada G, Balen
1027 RT, Beekman F, Ben-Avraham Z, Brun JP, Bunge HP, Burov EB, Carbonell R,
1028 Facenna C, Friedrich A, Gallart J, Green AG, Heidbach O, Jones AG, Matenco L,
1029 Mosar J, Oncken O, Pascal C, Peters G, Sliaupa S, Soesoo A, Spakman W,
1030 Stephenson RA, Thybo H, Torsvik T, de Vicente G, Wenzel F, Wortel MJR, TOPO-
1031 EUROPE Working Group 2 (2007) TOPO-EUROPE: The geoscience of coupled deep
1032 Earth-surface processes. Global and Planetary Change 58:1-118.
1033 Clynne MA, Borg LE (1997) Olivine and chromian spinel in primitive calc-alkaline and
1034 tholeiitic lavas from the southernmost Cascade Range, California; a reflection of
1035 relative fertility of the source. The Canadian Mineralogist 35:453-472.
1036 Condit CD, Connor CB (1996) Recurrence rates of volcanism in basaltic volcanic fields: An
1037 example from the Springerville volcanic field, Arizona. Geological Society of
1038 America Bulletin, 108:1225–1241
1039 Connor CB, Conway FM (2000) Basaltic Volcanic Fields. in: Sigurdsson H (Ed.)
1040 Encyclopedia of Volcanoes. Academic Press. San Diego pp 331-343.
1041 Courtillot V, Davaille A, Besse J, Stock J (2003) Three distinct types of hotspots in the
1042 Earth's mantle: Earth Planetary Science Letters, 205:295-308.

1043 Csontos L, Nagymarosy A, Horváth F, Kovác M, (1992) Tertiarry evolution of the intra-
1044 Carpathian area: a model. Tectonophysics, 208:221-241
1045 Dando BDE, Stuart GW, Houseman GA, Hegedűs E, Brückl E, Radovanovic S (2011)
1046 Teleseismic tomography of the mantle in the Carpathian-Pannonian region of central
1047 Europe. Geophysical Journal International, 186:11-31.
1048 Dasgupta R, Hirschmann MM, Stalker K (2006) Immiscible transition from carbonate-rich to
1049 silicate-rich melts in the 3 GPa melting interval of eclogite+CO3 and genesis of silica-
1050 undersaturated ocean island lavas. Journal of Petrology 47:647–671.
1051 Dasgupta R, Jackson MG, Lee CTA (2010) Major element chemistry of ocean island basalts -
1052 conditions of mantle melting and heterogeneity of mantle source. Earth and Planetary
1053 Science Letters 289:377-392.
1054 DePaolo DJ, Daley EE (2000) Neodymium isotopes in basalts of the southwest basin and
1055 range and lithospheric thinning during continental extension. Chemical Geology,
1056 169:157-185.
1057 Dérerova J, Zeyen H, Bielik M, Salman K (2006) Application of integrated geophysical
1058 modeling for determination of the continental lithospheric thermal structure in the
1059 eastern Carpathians. Tectonics, 25:TC3009. doi:10.1029/2005TC001883.
1060 Dick HJB, Bullen T (1984) Chromian spinel as a petrogenetic indicator in abyssal and alpine-
1061 type peridotites and spatially associated lavas. Contributions to Mineralogy and
1062 Petrology, 86:54-76.
1063 Dobosi G (1989) Clinopyroxene zoning patterns in the young alkali basalts of Hungary and
1064 their petrogenetic significance. Contributions to Mineralogy and Petrology, 101:112-
1065 121.

1066 Dobosi G, Fodor RV (1992) Magma fractionation, replenishment, and mixing as inferred
1067 from green-core clinopyroxenes in Pliocene basanite, southern Slovakia. Lithos
1068 28:133-150.
1069 Dobosi G, Fodor RV, Goldberg SA (1995) Late-Cenozoic alkali basalt magmatism in
1070 Northern Hungary and Slovakia: petrology, source compositions and relationship to
1071 tectonics. Acta Vulcanologica, 7:199-207.
1072 Dombrádi E, Sokoutis D, Bada G, Cloetingh S, Horváth F (2010) Modelling deformation of
1073 the Pannonian lithosphere: Lithospheric folding and tectonic topography.
1074 Tectonophysics, 484:103-118.
1075 Downes H, Seghedi I, Szakács A, Dobosi G, James DE, Vaselli O, Rigby IJ, Ingram GA, Rex
1076 D, Pécskay Z (1995) Petrology and geochemistry of late Tertiary/Quaternary mafic
1077 alkaline volcanism in Romania. Lithos, 35:65-81.
1078 Ellam RM (1992) Lithospheric thickness as a control on basalt geochemistry. Geology,
1079 20:153-156,
1080 Embey-Isztin A, Dobosi G (1995) Mantle source characteristics for Miocene-Pleistocene
1081 alkali basalts, Carpathian-Pannonian Region: A review of trace elements and isotopic
1082 composition. Acta Vulcanologica, 7:155-166.
1083 Embey-Isztin A, Dobosi G (2007) Composition of olivines in the young alkali basalts and
1084 their peridotite xenoliths from the Pannonian Basin. Annales Historico-Naturales
1085 Musei Nationalis Hungarici 99:5-22.
1086 Embey-Isztin A, Downes H, James DE, Upton BGJ, Dobosi G, Ingram GA, Harmon RS,
1087 Scharbert HG (1993) The petrogenesis of Pliocene alkaline volcanic rocks from the
1088 Pannonian Basin, Eastern Central Europe. Journal of Petrology 34:317-343.

1089 Embey-Isztin A, Dobosi G, Altherr R, Meyer HP (2001) Thermal evolution of the lithosphere
1090 beneath the western Pannonian Basin: evidence from deep-seated xenoliths.
1091 Tectonophysics 331:285-306.
1092 Erlund EJ, Cashman KV, Wallace, PJ, Pioli L, Rosi M, Johnson E, Granados HD (2010)
1093 Compositional evolution of magma from Parícutin Volcano, Mexico: The tephra
1094 record. Journal of Volcanology and Geothermal Research, 197:167-187.
1095 Fekiacova Z, Mertz DF, Hofmann AW (2007) Geodynamic setting of the Tertiary Hocheifel
1096 volcanism (Germany), Part II: Geochemistry and Sr, Nd and Pb isotopic compositions.
1097 In: Ritter J, Christensen U (Eds) Mantle Plumes - A Multidisciplinary Approach,
1098 Springer, pp. 207-239.
1099 Fisk MR, Bence AE (1980) Experimental crystallization of chrome spinel in FAMOUS basalt
1100 527-1-1. Earth and Planetary Science Letters 48:111-123.
1101 Fitton JG, James D, Kempton PD, Ormerod DS, Leeman WP (1988) The Role of Lithospheric
1102 Mantle in the Generation of Late Cenozoic Basic Magmas in the Western United
1103 States. Journal of Petrology Special Volume 1:331-349.
1104 Fitton JG, James D, Leeman WP (1991) Basic magmatism associated with Late Cenozoic
1105 extension in the Western United States: compositional variations in space and time.
1106 Journal of Geophysical Research, 96:13693-13711.
1107 Gazel E, Plank T, Forsyth DW, Bendersky C, Lee C, Hauri E (2012) Lithosphere vs.
1108 asthenosphere mantle sources at Big Pine Volcanic Field. Geochemistry, Geophysics,
1109 Geosystems, 13:doi:10.1029/2012GC004060
1110 Gîrbacea R, Frisch W (1998) Slab in the wrong place: Lower lithospheric mantle
1111 delamination in the last stage of Eastern Carpathians subduction retreat. Geology,
1112 26:611-614.

1113 Goes S, Spakman W, Bijwaard H (1999) A lower mantle source for central European
1114 volcanism, Science, 286:1928-1931.
1115 Granet M, Wilson M, Achauer U (1995) Imaging a mantle plume beneath the French Massif
1116 Central. Earth and Planetary Science Letters 136:281-296.
1117 Haase KM, Renno AD (2008) Variation of magma generation and mantle sources during
1118 continental rifting observed in Cenozoic lavas from the Eger Rift, Central Europe,
1119 Chemical Geology 257:195-205.
1120 Haase KM, Goldschmidt B, Garbe-Schönberg CD (2004) Petrogenesis of Tertiary continental
1121 intraplate lavas from the Westerwald region, Germany. Journal of Petrology 45:883-
1122 905.
1123 Halliday AN, Lee DC, Tommasini S, Davies GR, Paslick CR, Fitton JG, James DE (1995)
1124 Incompatible trace element in OIB and MORB source enrichment in the sub-oceanic
1125 mantle: Earth and Planetary Science Letters, v. 133, p. 379-395.
1126 Harangi S (2001a) Neogene to Quaternary Volcanism of the Carpathian-Pannonian Region - a
1127 review. Acta Geologica Hungarica. 44:223-258.
1128 Harangi S (2001b) Neogene magmatism in the Alpine-Pannonian Transition zone – a model
1129 for melt generation in a complex geodynamic setting. Acta Vulcanologica, 13:1-11.
1130 Harangi S. (2009): Volcanism of the Carpathian-Pannonian region, Europe: The role of
1131 subduction, extension and mantle plumes. MantlePlumes.org,
1132 http://www.mantleplumes.org/CarpathianPannonian.html, assessed 18 March 2014
1133 Harangi S, Lenkey L (2007) Genesis of the Neogene to Quaternary volcanism in the
1134 Carpathian-Pannonian region: Role of subduction, extension, and mantle plume.
1135 Geological Society of America Special Papers 418:67-92.

1136 Harangi S, Downes H, Thirlwall M, Gméling K (2007) Geochemistry, petrogenesis and
1137 geodynamic relationships of Miocene calc-alkaline volcanic rocks is the Western
1138 Carpathian Arc, eastern central Europe. Journal of Petrology, 48:2261-2287.
1139 Harangi S, Vaselli O, Tonarini S, Szabó C, Harangi R, Coradossi N (1995) Petrogenesis of
1140 Neogene extension-related alkaline volcanic rocks of the Little Hungarian Plain
1141 Volcanic Field (Western Hungary). Acta Vulcanologica, 7:173-187.
1142 Harangi S, Downes H, Seghedi I (2006) Tertiary-Quaternary subduction processes and related
1143 magmatism in the Alpine-Mediterranean region. In: Gee DG, Stephenson RA (eds)
1144 European Lithosphere Dynamics, Geological Society, London, Memoirs, 32:167-190.
1145 Harangi S, Ságí T, Seghedi I, Ntaflos T (2013) A combined whole-rock and mineral-scale
1146 investigation to reveal the origin of the basaltic magmas of the Perşani monogenetic
1147 volcanic field, Romania, eastern-central Europe. Lithos 180-181:43-57.
1148 Hart SR (1988) Heterogeneous mantle domains: signatures, genesis and mixing chronologies.
1149 Earth and Planetary Science Letters, 90:273-296.
1150 Herzberg C (2011) Identification of Source Lithology in the Hawaiian and Canary Islands:
1151 Implications for Origins. Journal of Petrology 52:113-146.
1152 Herzberg C, Asimow PD (2008) Petrology of some oceanic island basalts: PRIMELT2.XLS
1153 software for primary magma calculation. Geochemistry Geophysics Geosystem, 9,
1154 Q09001, doi:10.1029/2008GC002057.
1155 Hetényi G, Stuart G, Houseman G, Horvath F. Hegedüs E, Brückl E (2009) Anomalously
1156 deep mantle transition zone below Central Europe: evidence of lithospheric instability,
1157 Geophysical Research Letters, 36:doi: 10.1029/2009GL040171.
1158 Hill R, Roeder P (1974) The Crystallization of Spinel from Basaltic Liquid as a Function of
1159 Oxygen Fugacity. Journal of Geology 82:709-729.

1160 Hirose K, Kawamoto T (1995) Hydrous partial melting of lherzolite at 1 GPa - The effect of
1161 H_2O on the genesis of basaltic magmas. Earth and Planetary Science Letters 133:463-
1162 473.
1163 Hirose K, Kushiro I (1993) Partial melting of dry peridotites at high pressures: determination
1164 of composition of melts segregated from peridotite using aggregate of diamonds. Earth
1165 and Planetary Science Letters, 114:477-489.
1166 Hirschmann MM (2000) Mantle solidus: Experimental constraints and the effects of peridotite
1167 composition, Geochem. Geophys. Geosyst., 1, 1042:doi:10.1029/2000GC000070.
1168 Hirschmann MM (2006) Water, melting, and the deep Earth H_2O cycle. Annual Review of
1169 Earth and Planetary Sciences 34:629-653.
1170 Hirschmann MM, Tenner T, Aubaud C, Withers AC (2009) Dehydration melting of
1171 nominally anhydrous mantle: The primacy of partitioning. Physics of the Earth and
1172 Planetary Interiors 176:54-68.
1173 Hoernle K, Zhang YS, Graham D (1995) Seismic and geochemical evidence for large-scale
1174 mantle upwelling beneath the eastern Atlantic and western and central Europe. Nature
1175 374:34-39.
1176 Horváth F (1993) Towards a mechanical model for the formation of the Pannonian Basin.
1177 Tectonophysics 226:333-357.
1178 Horváth F, Cloetingh S (1996) Stress-induced late-stage subsidence anomalies in the
1179 Pannonian Basin. Tectonophysics 266:287-300.
1180 Horváth F, Faccenna C (2011) Central Mediterranean mantle flow system and the formation
1181 of the Pannonian basin. Geophysical Research Abstracts 13:EGU2011-8894-2.
1182 Horváth F, Dövényi P, Szalay, Á, Royden, L H. 1988. Subsidence, thermal and maturation
1183 history of the Great Hungarian Plain. In: Royden LH, Horváth F (eds) The Pannonian
1184 Basin: a Case Study in Basin Evolution. AAPG Memoirs, 45:355–372.

1185 Horváth F, Bada G, Szafián P, Tari G, Ádám A, Cloetingh S (2006) Formation and
1186 deformation of the Pannonian Basin. In: Gee DG, Stephenson RA (Eds.) European
1187 lithosphere dynamics. Geological Society London Memoirs, 32:191–207.
1188 Huismans RS, Podladchikov YY, Cloething S (2001) Dynamic modeling of the transition
1189 from passive to active rifting, application to the Pannonian basin. Tectonics 20:1021-
1190 1039.
1191 Humphreys ER, Niu Y (2009) On the composition of ocean island basalts (OIB): The effects
1192 of lithospheric thickness variation and mantle metasomatism. Lithos, 112:118-136.
1193 Hurai V, Danišík M, Huraiová M, Paquette JL, Ádám A. (2013) Combined U/Pb and (U-
1194 Th)/He geochronometry of basalt maars in Western Carpathians: implications for age
1195 of intraplate volcanism and origin of zircon metasomatism. Contributions to
1196 Minerology and Petrology, 166:1235-1251.
1197 Jankovics MÉ, Harangi S, Kiss B, Ntaflos T (2012) Open-system evolution of the Füzes-tó
1198 alkaline basaltic magma, western Pannonian Basin: Constraints from mineral textures
1199 and compositions. Lithos, 140-141:25-37.
1200 Jankovics MÉ, Dobosi G, Embey-Isztin A, Kiss B, Sági T, Harangi S, Ntaflos T (2013)
1201 Origin and ascent history of unusually crystal-rich alkaline basaltic magmas from the
1202 western Pannonian Basin. Bulletin of Volcanology, 75:1-23.
1203 Jung C, Jung S, Hoffer E, Berndt J (2006) Petrogenesis of Tertiary mafic alkaline magmas in
1204 the Hocheifel, Germany. Journal of Petrology 47:1637-1671.
1205 Jung S, Pfänder JA, Brügmann G, Stracke A. (2005) Sources of primitive alkaline rocks from
1206 the Central European Volcanic Province (Rhön, Germany) inferred from Hf, Os and
1207 Pb isotopes. Contributions to Mineralogy and Petrology, 150:546-559.
1208 Jung S, Vieten K, Romer RL, Mezger K, Hoernes S, Satir M (2012) Petrogenesis of Tertiary
1209 Alkaline Magmas in the Siebengebirge, Germany. Journal of Petrology 53:2381-2409.

1210 Kamenetsky, V.S, Crawford, A.J, Meffre, S, 2001. Factors controlling chemistry of magmatic
1211 spinel: an empirical study of associated olivine, Cr-spinel and melt inclusions from
1212 primitive rocks. Journal of Petrology 42, 655-671.
1213 Karato S (2011) Water distribution across the mantle transition zone and its implications for
1214 the global material circulation, Earth Planet. Sci. Lett., 301:413-423.
1215 Kawabata H, Hanyu T, Chang Q, Kimura JI., Nichols ARL, Tatsumi Y (2011) The Petrology
1216 and Geochemistry of St. Helena Alkali Basalts: Evaluation of the Oceanic Crust-
1217 recycling Model for HIMU OIB Journal of Petrology 52:791-838
1218 Kereszturi G, Németh K, Csillag G, Balogh K, Kovács J (2011) The role of external
1219 environmental factors in changing eruption styles of monogenetic volcanoes in a
1220 Mio/Pleistocene continental volcanic field in western Hungary. Journal of
1221 Volcanology and Geothermal Research 201:227-240.
1222 Kereszturi G, Németh K, Lexa J, Konecny V, Pécskay Z (2013) Eruptive volume estimate of
1223 the Nógrád-Gömör/Novohrad-Gemer Volcanic Field (Slovakia-Hungary). In Buecher
1224 J., Rapprich V, Tietz O. (Eds.) Abstract Volume & Excursion Guides - Basalt
1225 2013:168 - 169
1226 Klemme S, O'Neill HSC (2000) The near-solidus transition from garnet lherzolite to spinel
1227 lherzolite. Contributions to Mineralogy and Petrology 138:237-248
1228 Klemme S (2004) The influence of Cr on the garnet–spinel transition in the Earth's mantle:
1229 experiments in the system MgO–Cr2O3–SiO2 and thermodynamic modelling. Lithos,
1230 77:639–646.
1231 Kogiso T, Hirschmann MM, Frost DJ (2003) High-pressure partial melting of garnet
1232 pyroxenite: possible mafic lithologies in the source of ocean island basalts. Earth
1233 Planetary Science Letters 216:603-617.

1234 Kogiso T, Hirschmann MM (2006) Partial melting experiments of bimineralic eclogite and
1235 the role of recycled mafic oceanic crust in the genesis of ocean island basalts. Earth
1236 and Planetary Science Letters 249:188-199.
1237 Konečný V, Lexa J, Balogh K, Konečný P (1995) Alkali basalt volcanism in Southern
1238 Slovakia: volcanic forms and time evolution. Acta Volcanologica, 7:167-171.
1239 Konečný V, Lexa J, Balogh K (1999) Neogene-Quaternary alkali basalt volcanism in Central
1240 and Southern Slovakia (Western Carpathians). Geolines 9:67-75.
1241 Konečný V, Kováč M, Lexa J, Šefara J (2002) Neogene evolution of the Carpatho-Pannonian
1242 region: an interplay of subduction and back-arc diapiric uprise in the mantle. EGU
1243 Stephan Mueller Special Publication Series, 1:105-123.
1244 Kostopoulos, D.K, James, S.D. 1992. Parameterization of the melting regime of the shallow
1245 upper mantle and the effects of variable lithospheric stretching on mantle modal
1246 stratification and trace element concentrations in magmas. Journal of Petrology, 33,
1247 665-691.
1248 Kovács I, Falus G, Stuart G, Hidas K, Szabó C, Flower MFJ, Hegedűs E, Posgay K, Zilahi-
1249 Sebess L (2012) Seismic anisotropy and deformation patterns in upper mantle
1250 xenoliths from the central Carpathian-Pannonian region: Asthenospheric flow as a
1251 driving force for Cenozoic extension and extrusion? Tectonophysics, 514-517:168-
1252 179.
1253 Langmuir CH, Forsyth DW (2007) Mantle Melting Beneath Mid-Ocean Ridges.
1254 Oceanography 20:78–89
1255 Langmuir CH, Klein E, Plank T (1992) Petrological systematics of mid-ocean ridge basalts:
1256 Constraints on melt generation beneath ocean ridges. AGU Monograph, 71:183-280.

1257 Le Bas MJ, Le Maitre RW, Streckeisen A, Zanettin B (1986) A chemical classification of
1258 volcanic rocks based on the total alkali silica diagram. - Journal of Petrology, 27:745
1259 750.
1260 Lebedev S, Meier T, van der Hilst RD (2006) Asthenospheric flow and origin of volcanism in
1261 the Baikal Rift area. Earth & Planetary Science Letters, 249:415-424.
1262 Lee CT, Luffi P, Plank T, Dalton H, Leeman WP, (2009) Constraints on the depths and
1263 temperatures of basaltic magma generation on Earth and other terrestrial planets using
1264 new thermobarometers for mafic magmas. Earth and Planetary Science Letters
1265 279:20–33.
1266 Leloup PH, Lacassin R, Tapponnier P, Schärer U, Dalai Z, Xiaohan L, Liangshang Z,
1267 Shaocheng J, Trinh PT (1995) The Ailao Shan–Red River shear zone (Yunnan,
1268 China), Tertiary transform boundary of Indochina. Tectonophysics 251:3-84.
1269 Lenkey L, Dövényi P, Horváth F, Cloetingh S (2002) Geothermics of the Pannonian Basin
1270 and its bearing on the neotectonics. European Geophysical Union Stephan Mueller
1271 Special Publications, Series 3:29-40.
1272 Lexa J, Seghedi I, Németh K, Szakács A, Konečny V, Pécskay Z, Fülöp A, Kovacs M (2010)
1273 Neogene-Quaternary volcanic forms in the Carpathian-Pannonian Region: a review.
1274 Central European Journal of Geosciences 2: 207–270.
1275 Lorinczi P, Houseman GA (2010) Lithospheric gravitational instability beneath the Southeast
1276 Carpathians. Tectonophysics, 486:150-150.
1277 Luhr JF, Carmichael ISE (1985) Jorullo volcano, Michoacán, Mexico (1759–1774): The
1278 earlier stages of fractionation in calk-alkaline magmas. Contributions to Mineralogy
1279 and Petrology, 90:142–161
1280 Lustrino M, Wilson M (2007) The Circum-Mediterranean Anorogenic Cenozoic Igneous
1281 Province. Earth-Science Reviews, 81:1–65.

1282 Ma GSK, Malpas J, Xenophontos C, Chan GHN (2011) Petrogenesis of latest
1283 Miocene^Quaternary continental intraplate volcanism along the northern Dead Sea
1284 Fault System (Al Ghab-Homs volcanic field), western Syria: evidence for lithosphere-
1285 asthenosphere interaction. Journal of Petrology 52:401-430.
1286 Martin U, Németh K (2004) Mio/Pliocene Phreatomagmatic Volcanism in the Western
1287 Pannonian Basin: Budapest, Geological Institute of Hungary, 193 p.
1288 Martin M, Wenzel F, CALIXTO Working Group (2006) High-resolution teleseismic body
1289 wave tomography beneath SE Romania: II. Imaging of a slab detachment scenario.
1290 Geophysical Journal International, 164:579–595.
1291 Mayer B, Jung S, Romer RL, Stracke A, Haase KM, Garbe-Schönberg CD. (2013)
1292 Petrogenesis of Tertiary Hornblende-bearing Lavas in the Rhön, Germany. Journal of
1293 Petrology, 54:2095-2123.
1294 Mayer B, Jung S, Romer R, Pfänder JA, Klügel A, Pack A, Gröner E. (2014) Amphibole in
1295 alkaline basalts from intraplate settings: implications for the petrogenesis of alkaline
1296 lavas from the metasomatised lithospheric mantle. Contributions to Mineralogy and
1297 Petrology, 167:DOI: http://doi.org/10.1007/s00410-014-0989-3
1298 McDonough WF, Sun SS (1995) The composition of the Earth. Chemical Geology, 120:223-
1299 253.
1300 McGee LE, Millet MA, Smith IEM, Németh K, Lindsay JM (2012) The inception and
1301 progression of melting in a monogenetic eruption: Motukorea Volcano, the Auckland
1302 Volcanic Field, New Zealand. Lithos 155:360-374.
1303 McGee LE, Smith IEM, Millet MA, Handley HK, Lindsay JM (2013) Asthenospheric Control
1304 of Melting Processes in a Monogenetic Basaltic System: a Case Study of the Auckland
1305 Volcanic Field, New Zealand. Journal of Petrology 54:2125-2153.

McKenzie D (1989) Some remarks on the movement of small melt fractions in the mantle: Earth Planetary Science Letters, 95:53-72.

Niu Y (2005) Generation and evolution of basaltic magmas: Some basic concepts and a hypothesis for the origin of the Mesozoic-Cenozoic volcanism in eastern China, Geological Journal of China Universities, 11:9-46.

Niu Y (2008) The origin of alkaline lavas. Science, 320:883-884.

Niu Y, Wilson M, Humphreys ER, O'Hara MJ (2011) The Origin of Intra-plate Ocean Island Basalts (OIB): the Lid Effect and its Geodynamic Implications. Journal of Petrology, 52:1443-1468

Ormerod DS, Rogers NW, Hawkesworth CJ (1991) Melting in the lithospheric mantle: Inverse modelling of alkali-olivine basalts from the Big Pine Volcanic Field, California. Contributions to Mineralogy and Petrology, 108:305-317.

Panaiotu CG, Jicha BR, Singer BS, Tugui A, Seghedi I, Panaiotu AG, Necula C (2013) 40Ar/39Ar chronology and paleomagnetism of Quaternary basaltic lavas from the Perşani Mountains (East Carpathians). Physics of the Earth and Planetary Interiors, 221:1-24.

Panaiotu CG, Pécskay Z, Hambach U, Seghedi I, Panaiotu CE, Tetsumaru I, Orleanu M, Szakács A (2004) Short-lived Quaternary volcanism in the Persani Mountains (Romania) revealed by combined K-Ar and paleomagnetic data. Geologica Carpathica, 55:333-339.

Pertermann M, Hirschmann MM (2003) Partial melting experiments on a MORB-like pyroxenite between 2 and 3 GPa: Constraints on the presence of pyroxenite in basalt source regions from solidus location and melting rate. Journal of Geophysical Research: Solid Earth, 108(B2):2125:doi:10.1029/2000JB000118

1330 Pilet S, Hernandez J, Sylvester P, Poujol M (2005) The metasomatic alternative for ocean
1331 island basalt chemical heterogeneity: Earth and Planetary Science Letters, 236:148-
1332 166.
1333 Pilet S, Baker MB, Stolper EM (2008) Metasomatized lithosphere and the origin of alkaline
1334 lavas. Science, 320:916-919.
1335 Piromallo C, Morelli A (2003) P wave tomography of the mantle under the Alpine-
1336 Mediterranean area, Journal of Geophysical Research, 108:doi:
1337 10.1029/2002JB001757
1338 Piromallo C, Vincent AP, Yuen DA, Morelli A (2001) Dynamics of the trasition zone under
1339 Europe inferred from wavelet cross-spectra of seismic tomography. Physics of the
1340 Earth and Planetary Inferiors, 125:125-139.
1341 Popa M, Radulian M, Szakács A, Seghedi I, Zaharia B (2012) New Seismic and Tomography
1342 Data in the Southern Part of the Harghita Mountains (Romania, Southeastern
1343 Carpathians): Connection with Recent Volcanic Activity. Pure Appl. Geophys,
1344 169:1557-1573.
1345 Putirka KD, Kuntz MA, Unruh DM, Vaid N (2009) Magma Evolution and Ascent at the
1346 Craters of the Moon and Neighboring Volcanic Fields, Southern Idaho, USA:
1347 Implications for the Evolution of Polygenetic and Monogenetic Volcanic Fields.
1348 Journal of Petrology, 50:1639-1665.
1349 Robinson JA, Wood BJ (1998) The depth of the spinel to garnet transition at the peridotite
1350 solidus. Earth Planetary of Science Letters, 164:277–284.
1351 Roeder PL, Reynolds I (1991) Crystallization of Chromite and Chromium Solubility in
1352 Basaltic Melts. Journal of Petrology 32:909-934.

1353 Roeder PL, Thornber C, Poustovetov A, Grant A (2003) Morphology and composition of
1354 spinel in Pu'u 'O'o lava (1996-1998), Kilauea volcano, Hawaii. Journal of Volcanology
1355 and Geothermal Research 123:245-265.
1356 Roeder P, Gofton E, Thornber C (2006) Cotectic proportions of olivine and spinel in olivine-
1357 tholeiitic basalt and evaluation of pre-eruptive processes. Journal of Petrology, 47:883-
1358 900.
1359 Royden LH, Horváth F, Burchfiel BC (1982) Transform faulting, extension and subduction in
1360 the Carpathian-Pannonian region: Geological Society of America Bullettin, 93:717-
1361 725.
1362 Rudnick RL, Fountain DM (1995) Nature and composition of the continental crust: a lower
1363 crustal perspective. Reviews of Geophysics, 33:267–309.
1364 Sági T, Harangi S (2013) Origin of the magmas in the Late Miocene to Quaternary Nógrád-
1365 Selmec mongenetic alkali basalt volcanic field, southern-central Slovakia. in : Büchner
1366 J, Rapprich V, Tietz O. (eds) Basalt 2013 Conference Abstract and Excursion Guides,
1367 Görlitz, Germany:17-18.
1368 Sakuyama T, Ozawa K, Sumino H, Nagao K (2009) Progressive melt extraction from
1369 upwelling mantle constrained by the Kita-Matsuura Basalts in NW Kyushu, SW
1370 Japan. Journal of Petrology, 50:725-779.
1371 Salters VJM, Hart SR (1989) The hafnium paradox and the role of garnet in the source of
1372 mid-ocean-ridge basalts. 342:420-422.
1373 Salters VJM, Stracke A (2004) Composition of the depleted mantle. Geochemistry,
1374 Geophysics, Geosystems, 5:Q05B07, doi:10.1029/2003GC000597.
1375 Scarrow JH, Cox KG (1995) Basalts generated by decompressive adiabatic melting of a
1376 mantle plume: a case study from the Isle of Skye, NW Scotland. Journal of Petrology,
1377 36:3-22.

1378 Sclater J, Royden L, Horváth F, Burchfiel B, Semken S, Stegena L. (1980) The formation of
1379 the intra-Carpathian basins as determined from subsidence data. Earth and Planetary
1380 Science Letters, 51:139–162.
1381 Seghedi I, Szakács A (1994) The Upper Pliocene-Pleistocene effusive and explosive basaltic
1382 volcanism from the Perşani Mountains. Rom. J. Petrology 76:101-107.
1383 Seghedi I, Downes H (2011) Geochemistry and tectonic development of Cenozoic
1384 magmatism in the Carpathian–Pannonian region. Gondwana Research 20:655-672.
1385 Seghedi I, Balintoni I, Szakács A (1998) Interplay of tectonics and neogene post-collisional
1386 magmatism in the intracarpathian region. Lithos, 45:483-497.
1387 Seghedi I, Downes H, Szakacs A, Mason PRD, Thirlwall MF, Rosu E, Pecskay Z, Marton E,
1388 Panaiotu C (2004a) Neogene-Quaternary magmatism and geodynamics in the
1389 Carpathian-Pannonian region: a synthesis. Lithos, 72:117-146.
1390 Seghedi I, Downes H, Vaselli O, Szakács A, Balogh K, Pécskay Z (2004b) Post-collisional
1391 Tertiary-Quaternary mafic alkalic magmatism in the Carpathian-Pannonian region: a
1392 review. Tectonophysics 393:43-62.
1393 Seghedi I, Downes H, Harangi S, Mason PRD, Pecskay Z (2005) Geochemical response of
1394 magmas to Neogene-Quaternary continental collision in the Carpathian-Pannonian
1395 region: A review. Tectonophysics, 410:485-499.
1396 Seghedi I, Mațenco L, Downes H, Mason PRD, Szakács A, Pécskay Z (2011) Tectonic
1397 significance of changes in post-subduction Pliocene-Quaternary magmatism in the
1398 south east part of the Carpathian-Pannonian Region. Tectonophysics, 502:146-157.
1399 Shaw DM (1970) Trace element fractionation during anatexis. Geochimica et Cosmochimica
1400 Acta, 34:237-243.
1401 Shaw DM (2000): Continuous (dynamic) melting theory revisited. The Canadian Mineralogist
1402 38:1041-1063

1403 Sigurdsson H, Schilling JG (1976) Spinels in Mid-Atlantic Ridge basalts: Chemistry and
1404 occurrence. Earth and Planetary Science Letters 29:7-20.
1405 Šimon L, Halouzka R (1996) Pútikov vrsok volcano - the youngest volcano in the Western
1406 Carpathians. Slovak Geological Magazine, 2:103-123.
1407 Šimon L, Maglay J (2005) Dating of sediments underlying the Putikov vŕšok volcano lava
1408 flow by the OSL method. Miner. Slovaca 37:279-281.
1409 Smith IEM, Blake S, Wilson CJN, Houghton BF (2008) Deep-seated fractionation during the
1410 rise of a small-volume basalt magma batch: Crater Hill, Auckland, New Zealand.
1411 Contributions to Mineralogy and Petrology, 155:511-527.
1412 Sobolev AV, Shimizu N (1992) Ultradepleted Melts and the Permeability of the Oceanic
1413 Mantle. Dokl. Ross. Akad. Nauk 326:354–360
1414 Sobolev AV, Hofmann AW, Sobolev SV, Nikogosian IK (2005) An olivine-free mantle
1415 source of Hawaiian shield basalts. Nature, 434:590-597.
1416 Sobolev AV, Hofmann AW, Kuzmin DV, Yaxley GM, Arndt NT, Chung SL, Danyushevsky
1417 LV, Elliott T, Frey FA, Garcia MO, Gurenko AA, Kamenetsky VS, Kerr AC,
1418 Krivolutskaya NA, Matvienkov VV, Nikogosian IK, Rocholl A, Sigurdsson IA,
1419 Sushchevskaya NM, Teklay M (2007) The amount of recycled crust in sources of
1420 mantle-derived melts. Science, 316:412-417.
1421 Späth A, Le Roex AP, Opiyo-Akech N. (2001) Plume-Lithosphere Interaction and the Origin
1422 of Continental Rift-related Alkaline Volcanism - the Chyulu Hills Volcanic Province,
1423 Southern Kenya. Journal of Petrology 42:765-787.
1424 Sperner B, Lorenz F, Bonjer K, Hettel S, Muller B, Wenzel F (2001) Slab break-off - abrupt
1425 cut or gradual detachment? New insights from the Vrancea Region (SE Carpathians,
1426 Romania). Terra Nova, 13:172-179.

1427 Sperner B, Ioane D, Lillie RJ (2004) Slab behaviour and its surface expression: new insights
1428 from gravity modelling in the SE-Carpathians. Tectonophysics, 382:51-84.
1429 Stegena L, Géczy B, Horváth F (1975) Late Cenozoic evolution of the Pannonian basin -
1430 Tectonophysics 26:71-90.
1431 Stracke A, Hofmann AW, Hart SR (2005) FOZO, HIMU and the rest of the mantle zoo.
1432 Geochemistry, Geophysics, Geosystems 6:doi:10.1029/2004GC000824.
1433 Strong M, Wolff J (2003) Compositional variations within scoria cones. Geology 31:143-146.
1434 Sun, S, McDonough, W.F, 1989. Chemical and isotopic systematics of oceanic basalts:
1435 implications for mantle compositions and processes. Geological Society Special
1436 Publication, 42, 313-345.
1437 Szabó C, Harangi S, Csontos L (1992) Review of Neogene and Quaternary volcanism of the
1438 Carpathian-Pannonian region. Tectonophysics, 208:243-256.
1439 Szabó C, Falus G, Zajacz Z, Kovács I, Bali E (2004) Composition and evolution of
1440 lithosphere beneath the Carpathian-Pannonian Region: a review. Tectonophysics, 393:
1441 119-137.
1442 Takahashi E, Kushiro I (1983) Melting of a dry peridotite at high pressures and basalt magma
1443 genesis. American Mineralogist, 68:859-879.
1444 Tari G, Dövényi P, Horváth F, Dunkl I, Lenkey L, Stefanescu M, Szafián P, Tóth T (1999).
1445 Lithospheric structure of the Pannonian Basin derived from seismic, gravity and
1446 geothermal data. in: Durand B, Jolivet L, Horváth F, Séranne M. (Eds.) The
1447 Mediterranean Basins: Tertiary extension within the Alpine orogen. Geological
1448 Society, London, Special Publication, 156, pp. 215-250.
1449 Timm C, Hoernle K, van den Bogaard P, Bindeman I, Weaver S (2009) Geochemical
1450 evolution of intraplate volcanism at Banks Peninsula, New Zealand: interaction
1451 between asthenospheric and lithospheric melts. Journal of Petrology 50:989-1023.

1452 Timm C, Hoernle K, Werner R, Hauff F, van den Bogaard P, White J, Mortimer N, Garbe-
1453 Schönberg D (2010) Temporal and geochemical evolution of the Cenozoic intraplate
1454 volcanism of Zealandia. Earth-Science Reviews 98:38-64.
1455 Tschegg C, Ntaflos T, Kiraly F, Harangi S (2010) High temperature corrosion of olivine
1456 phenocrysts in Pliocene basalts from Banat, Romania. Austrian Journal of Earth-
1457 Sciences, 103:101-110.
1458 Valentine GA, Perry FV (2007) Tectonically controlled, time-predictable basaltic volcanism
1459 from a lithospheric mantle source (central Basin and Range Province, USA). Earth and
1460 Planetary Science Letters, 261:201-216.
1461 Vauchez A, Tommasi A, Mainprice, D (2012) Faults (shear zones) in the Earth's mantle.
1462 Tectonophysics, 558-559:1-27.
1463 Wallace M, Green DH (1991) The effect of bulk rock composition on the stability of
1464 amphibole in the upper mantle: Implications for solidus positions and mantle
1465 metasomatism. Mineralogy and Petrology, 44:1-19
1466 Walter MJ (1998) Melting of garnet peridotite and the origin of komatiite and depleted
1467 lithosphere. J. Petrol. 39:29–60.
1468 Wang K, Plank T, Walker JD, Smith EI (2002) A mantle melting profile across the Basin and
1469 Range, SW USA. Journal of Geophysical Research: Solid Earth, 107(B1):ECV 5-1-
1470 ECV 5-21.
1471 Wijbrans J, Németh K, Martin U, Balogh K (2007) 40Ar/39Ar geochronology of Neogene
1472 phreatomagmatic volcanism in the western Pannonian Basin, Hungary. Journal of
1473 Volcanology and Geothermal Research 164:193-204.
1474 Wilson M, Bianchini G (1999) Tertiary-Quaternary magmatism within the Mediterranean and
1475 surrounding regions. in: Durand B, Jolivet L, Horváth F, Séranne M (eds) The

Mediterranean Basins: Tertiary extension within the Alpine orogen, Geological Society London Special Publication, 156, pp. 141-168.

Wilson M, Downes H (1991) Tertiary-Quaternary extension-related alkaline magmatism in Western and Central Europe. Journal of Petrology, 32:811-849.

Wilson M, Downes H (2006) Tertiary-Quaternary intra-plate magmatism in Europe and its relationship to mantle dynamics, In: Stephenson R; Gee D (Ed) European Lithosphere Dynamics, Geological Society of London Memoir, 32:147-166.

Wilson M, Patterson R. (2001) Intraplate magmatism related to short-wavelength convective instabilities in the upper mantle: Evidence from the Tertiary-Quaternary volcanic province of western and central Europe. In: Ernst RE, Buchan KL (Eds) Mantle Plumes: Their Identification Through Time. Geol. Soc. Amer. Spec. Paper, 352:37-58.

Woodland AB, Jugo PJ (2007) A complex magmatic system beneath the Devés volcanic field, Massif Central, France: evidence from clinopyroxene megacrysts. Contributions to Mineralogy and Petrology 153:719-731.

Wortel MJR, Spakman W (2000) Subduction and Slab Detachment in the Mediterranean-Carpathian Region. Science, 290:1910-1917.

Zou H (1998) Trace element fractionation during modal and nonmodal dynamic melting and open-system melting; a mathematical treatment. Geochim. Cosmochim. Acta 62:1937-1945.

Figure captions

Figure 1. – (A) Geological setting and (B) location of the Miocene to Quaternary basalts in the Carpathian-Pannonian Region with the main tectonic lines (after Horváth et al., 2006). SVF=Styrian Volcanic Field; BU=Burgenland basalts; KVF=Kemenes Volcanic Field; BBVF=Bakony-Balaton Upland Volcanic Field; ST= Štiavnica basalts; KE=Kecel basalts (buried); LU=Lucaret basalt; PVF=Perşani Volcanic Field.

Figure 2. – Classification of the basalts based on the TAS diagram (Le Bas et al. 1986). The used data set is found in the supplementary table along with the references to the sources of the data. Data of the Pásztori trachyte is from Harangi et al. (1995) and Harangi (2001b).

Figure 3. - Selected major elements (in wt%) and trace elements (in ppm) vs. MgO for the CPR basalts. Symbols as in Fig. 2.

Figure 4. – Primitive mantle (McDonough and Sun, 1995) normalized trace element patterns for representative CPR basalts. Note that two groups can be distinguished based on the incompatible trace element abundances and the existence of negative K-anomaly.

Figure 5. – $(La/Yb)_N$ vs. K/K* and $^{143}Nd/^{144}Nd$ vs. K/K* diagrams for the CPR basalts. Note the negative correlation between these variables suggesting formation of the strongest negative K-anomaly in the melts generated at small degree of melting where garnet remained in the residue. The covariance between $^{143}Nd/^{144}Nd$ and K/K* in the different basalt volcanic fields of the CPR implies that the negative K-anomaly could be inherited in the mantle source regions. The K/K* is calculated as $K_N/\sqrt{(Nb_N*La_N)}$, where N denotes normalization to the primitive mantle (McDonough and Sun, 1995) values. Symbols as in Fig. 2.

Figure 6. – (A) Estimation of the initial and final pressures (p_o and p_f, respectively) of the melting column for selected CPR basalts using the adiabatic decompression model of Langmuir et al. (1992). The FeO^t and the Na_2O of the calculated primary magmas of the CPR basalts yield information on the initial melting pressure and the cessation of the melting, i.e. the final melting pressure. Each curve represents polybaric mantle melting lines with different initial melting pressure, i.e. where the ambient mantle temperature intersects the solidus. Each tick mark represents 0.1 GPa of decompression. The compositions of the primary magmas at the melting curves provide the values of the final pressure.

(B) Determination of melting pressure based on the calculated primary magma compositions of the CPR basalts using the ol'-ne'-qtz' plot of Hirose and Kushiro (1993). ol'=ol+0.75opx; ne'=ne+0.6ab; qtz'=qtz+0.4ab+0.25opx, where ol, opx, ne, ab, qtz are CIPW normative mineral components. Melting pressure lines are after Sakuyama et al. (2009).

Figure 7. – Calculated melting columns for different basalts (based on Langmuir et al., 1992 model) compared with the present lithosphere-asthenpshere boundary (LAB) beneath the volcanic fields that is inferred from interpretation of seismic data (Horváth et al., 2006). Mantle potential temperatures are given using the calculation scheme of Lee et al. (2009) using molar Fe^{3+}/Fe^{tot}=0.13. Beneath the Perşani volcanic field Dérerova et al. (2006) and Horváth et al. (2006) suggested a thick lithosphere (about 140 km), whereas Martin et al. (2006) indicated much thinner lithosphere. Our melting column calculation for the Perşani basalts is consistent with the proposed lithosphere thickness of Martin et al. (2006).

Figure 8. – Comparison of the melting pressure obtained by the calculation procedure of Lee et al. (2009) with the final melting pressure (p_f) provided by the Langmuir et al. (1992)

model. There is a reasonably good correlation between these pressure values. Symbols as in Fig. 2.

Figure 9. - Trace element modelling for the melt generation of the CPR basaltic magmas. Model parameters: critical melting model (critical melt fraction is 0.01) proposed by Sobolev and Shimizu (1992) with the following source rocks: spinel-lherzolite – olivine (57%), orthopyroxene (25.5%), clinopyroxene (15%), spinel (2.5%); garnet-lherzolite - olivine (60.1%), orthopyroxene (18.9%), clinopyroxene (13.7%), garnet (7.3%). Melting modes are ol1.21opx8.06cpx76.37sp14.36 for sp-lherzolite and ol1.3opx8.7cpx36gt54 for garnet-lherzolite, respectively. Source rock composition: La and Nb - 4 x primitive mantle values (2.59 and 2.63 ppm, respectively), Zr - 2 x primitive mantle values (21 ppm) and Y – 1.5 x primitive mantle values (6.45 ppm, where primitive mantle values are from McDonough and Sun, 1995). Distribution coefficients are from Kostopoulos and James (1992). Tick marks indicate the degree of melting at each melting model. Symbols are explained in Fig. 2.

Figure 10. – Melting conditions beneath the Carpathian-Pannonian region in a pressure-temperature diagram. The position of the melting columns is based on the result of the Langmuir et al. (1992) model combined with the mantle potential temperature and melting pressure values calculated by the thermbarometer of Lee et al. (2009). The melting columns of the basaltic magmas are just below the dry peridotite solidus (as defined by Hirschmann, 2000). This requires either some water or a more fusible material, such as pyroxenite or eclogite in the mantle source. Hydrous peridotite solidi: Hirschmann (2006); pyroxenite (MIX1G) pyroxenite solidus: Kogiso et al. (2003); MORB-like pyroxenite solidus: Pertermann and Hirschmann (2003). UMX: position of the ultramafic peridotite xenoliths as given by Embey-Isztin et al. (2001) and Kovács et al. (2012).

1570 Figure 11. - Compositional characteristics of spinel inclusions in olivine phenocrysts of the
1571 CPR basalts based on the Cr-Fe^{3+}-Al diagram. The most primitive spinels form four
1572 compositionally coherent groups that can be related to the existence of different
1573 mantle domains in the source regions of the basaltic magmas. Note that three of these
1574 groups are present beneath each volcanic fields of the CPR. MORB and OIB spinel
1575 fields are as defined by Barnes and Roeder (2001). Compositional data of spinels are
1576 from Jankovics et al. (2012), Harangi et al. (2013) and Sági et al. (in prep).
1577 Figure 12. – Position of the basalt volcanic fields in the CPR compared with the seismically
1578 defined lithosphere-asthenosphere boundary lines (Horváth et al., 2006). Note that the
1579 volcanic fields are located at the margin of the Pannonian basin and not in the central
1580 parts where the lithosphere is the thinnest.
1581 Figure 13. – Conceptual model for the triggering of melt generation beneath the Pannonian
1582 basin. See text for explanation.
1583
1584 Table 1 – Representative major and trace element composition of the basalts from different
1585 volcanic fields of the CPR. Reference: 1: Ali et al. (2013), 2: Ali and Ntaflos (2011),
1586 3: this study, 4: Harangi et al. (2013). p_f and p_o are the calculated final and initial
1587 melting pressures using the Langmuir et al. (1992) model. T and p are the mantle
1588 potential temperature and the melting pressure using the thermobarometer of Lee et al.
1589 (2009) with molar Fe^{3+}/Fe^{tot}=0.13.

Figure 1A

Click here to download high resolution image

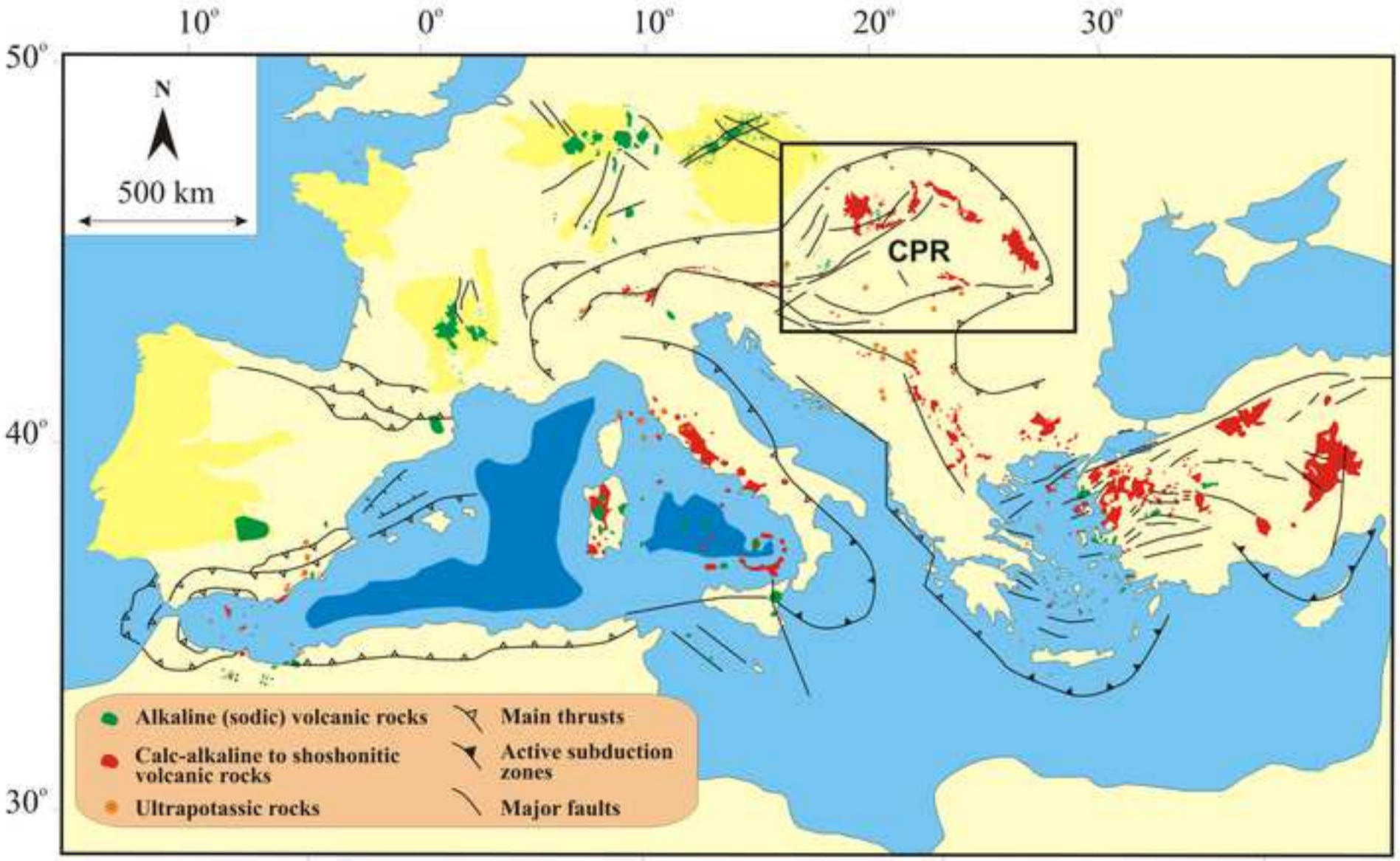

Figure 1B
Click here to download high resolution image

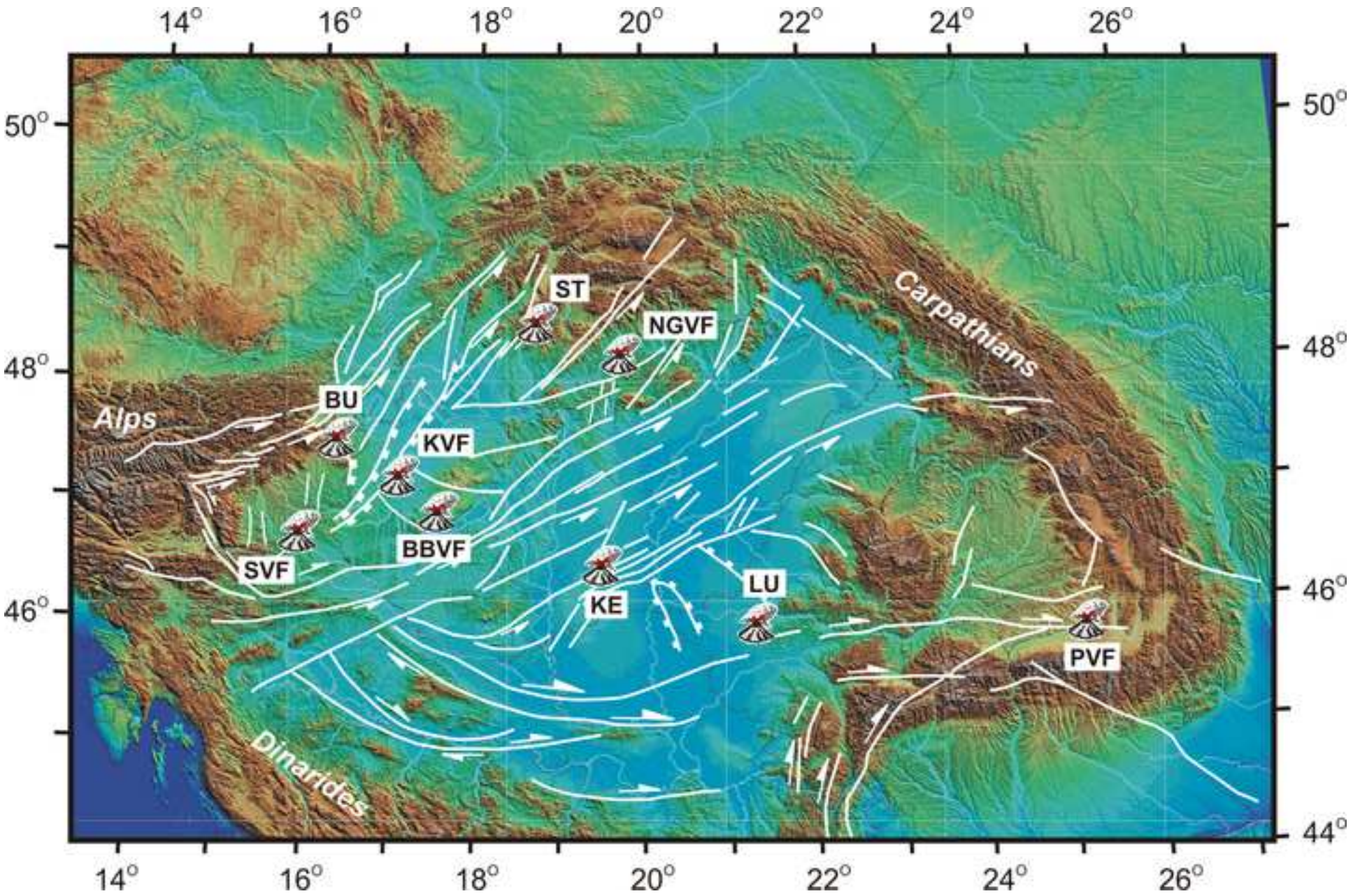

Figure 2
Click here to download high resolution image

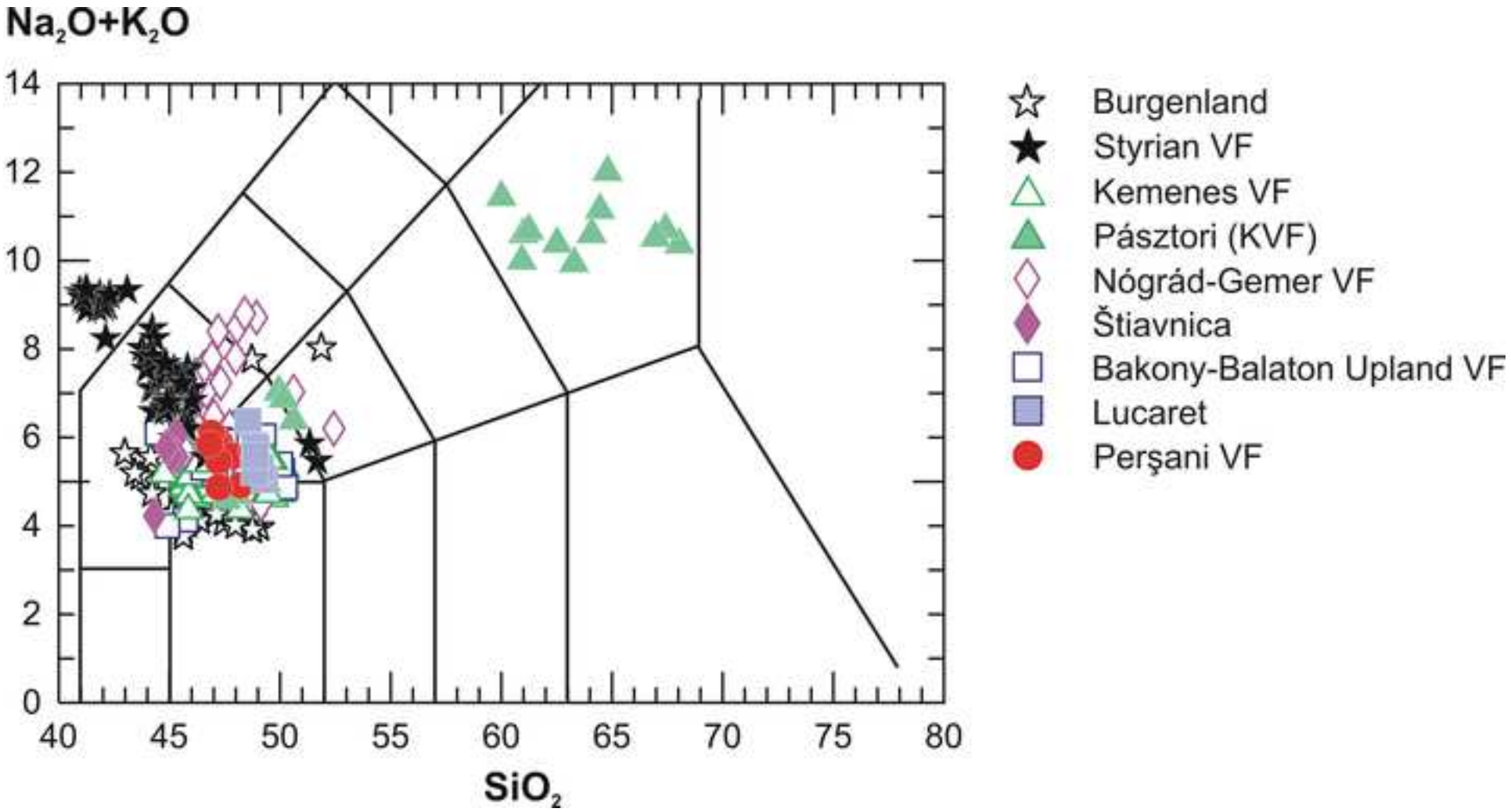

Figure 3

Click here to download high resolution image

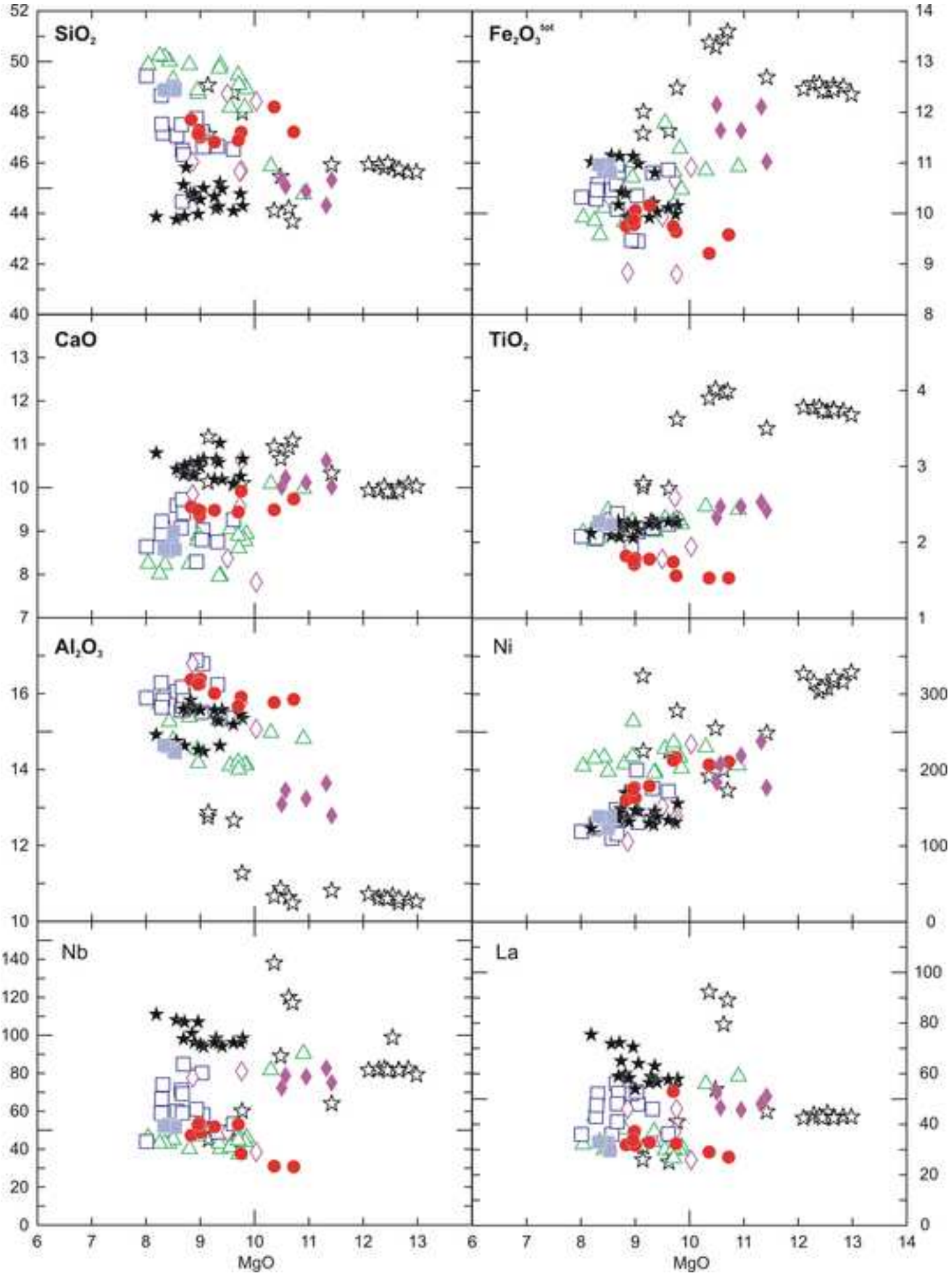

Figure 4
Click here to download high resolution image

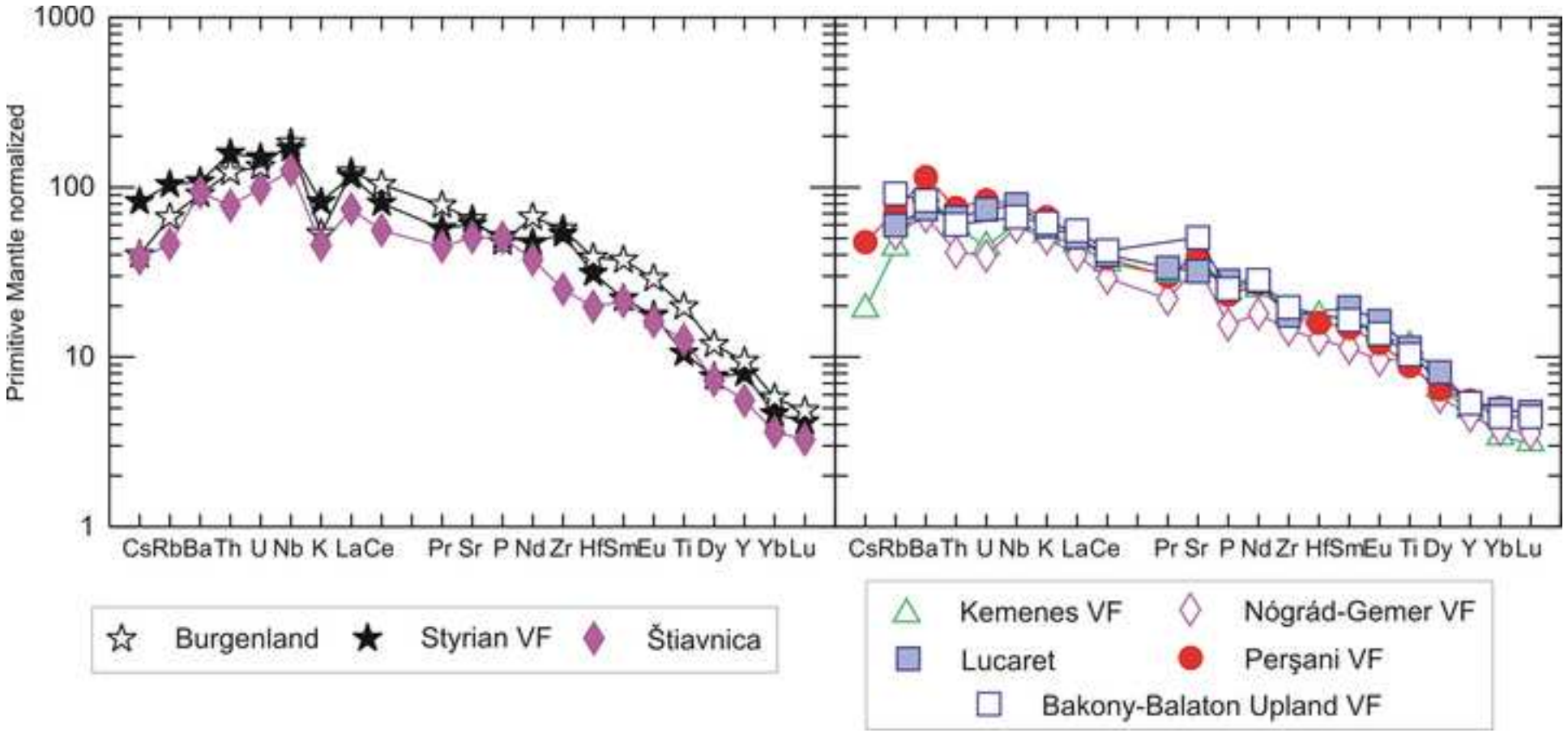

Figure 5
Click here to download high resolution image

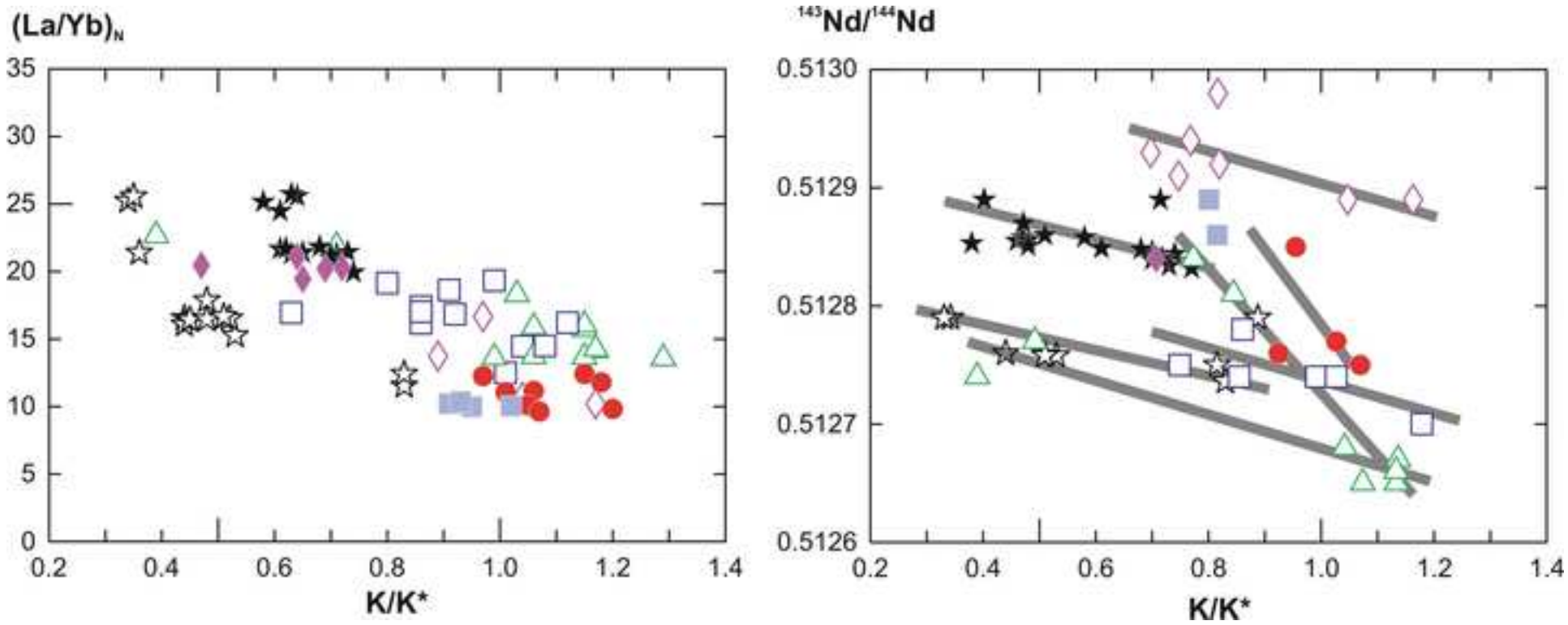

Figure 6A
Click here to download high resolution image

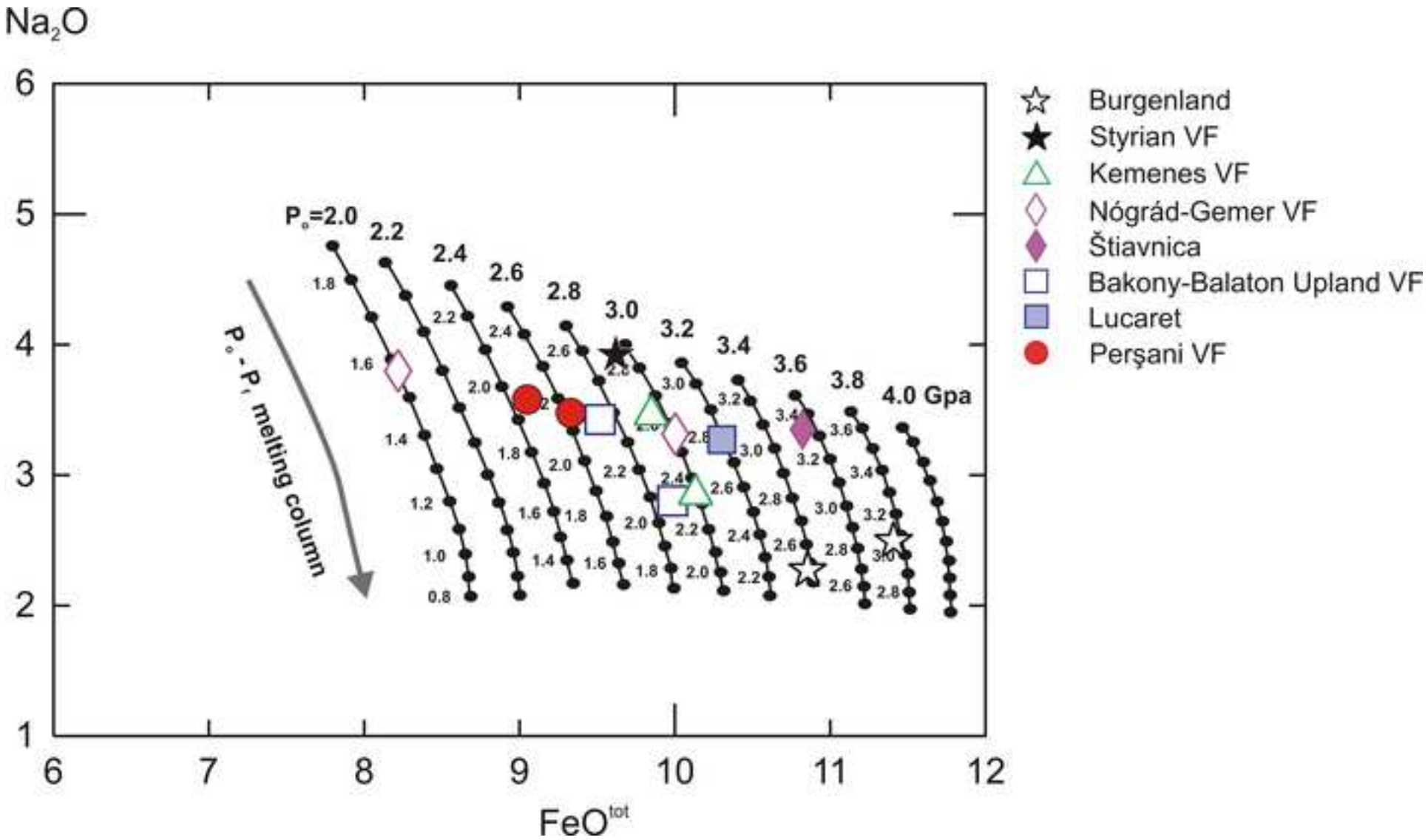

Figure 6B
Click here to download high resolution image

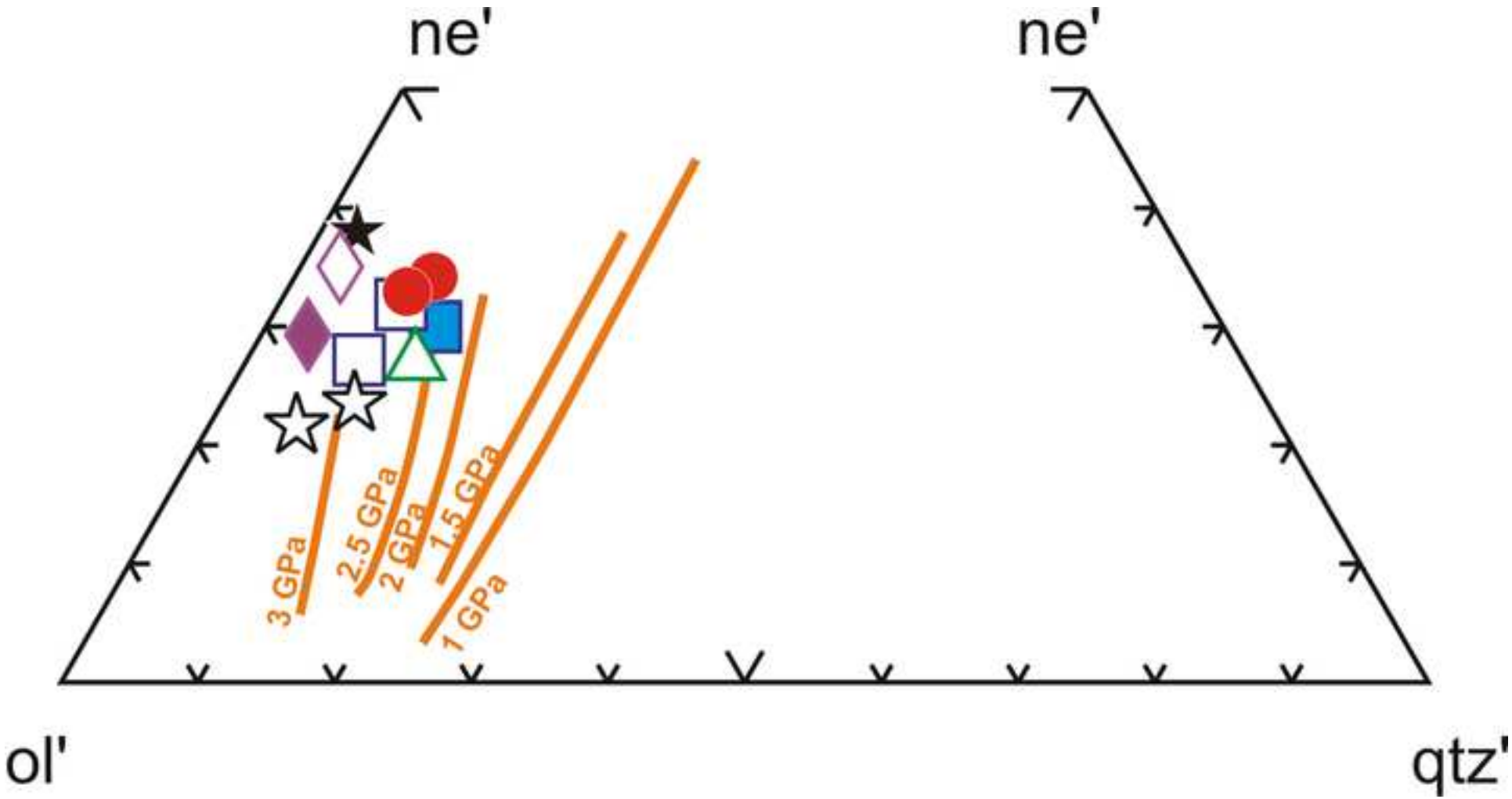

Figure 7
Click here to download high resolution image

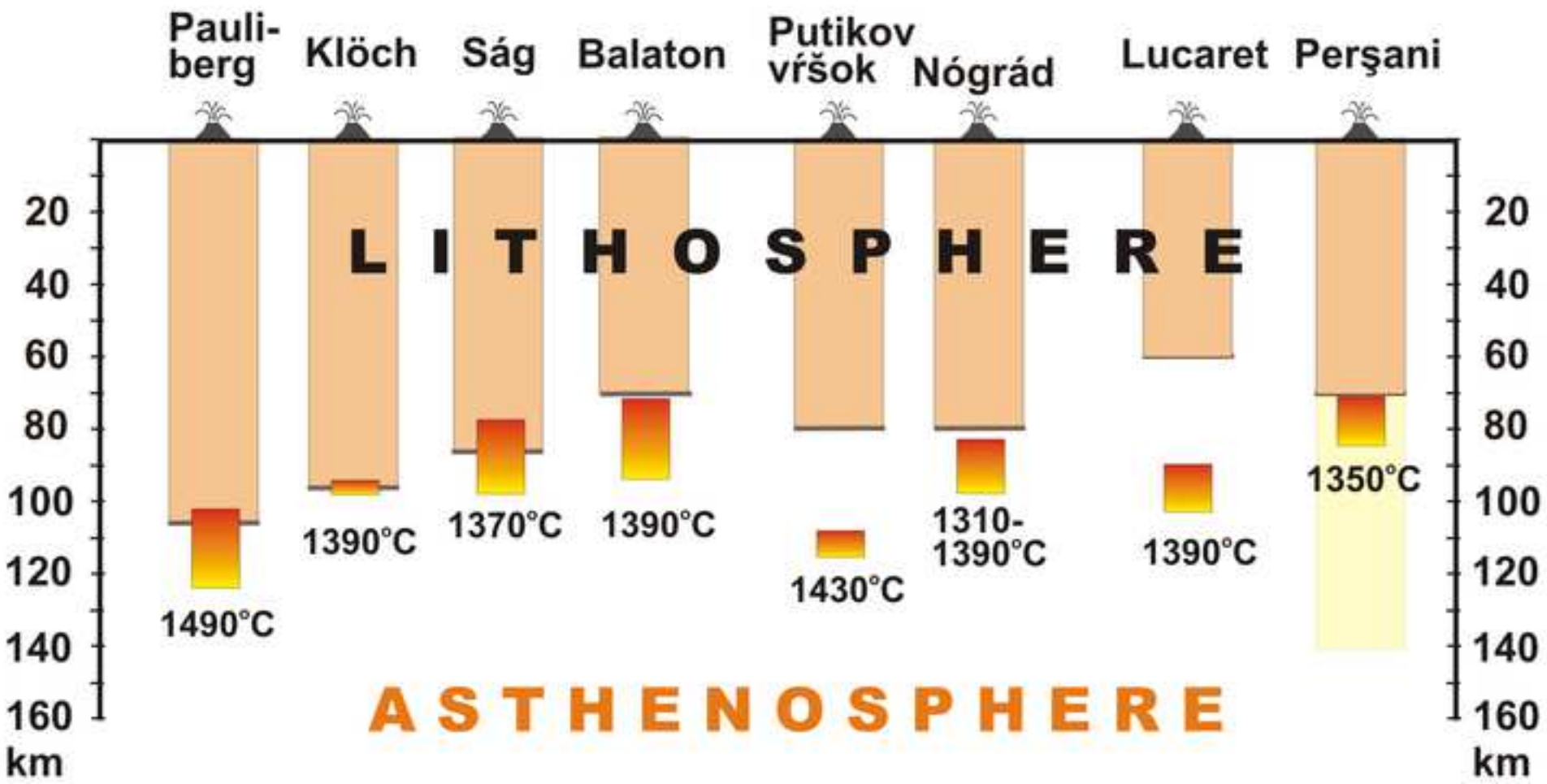

Figure 8
Click here to download high resolution image

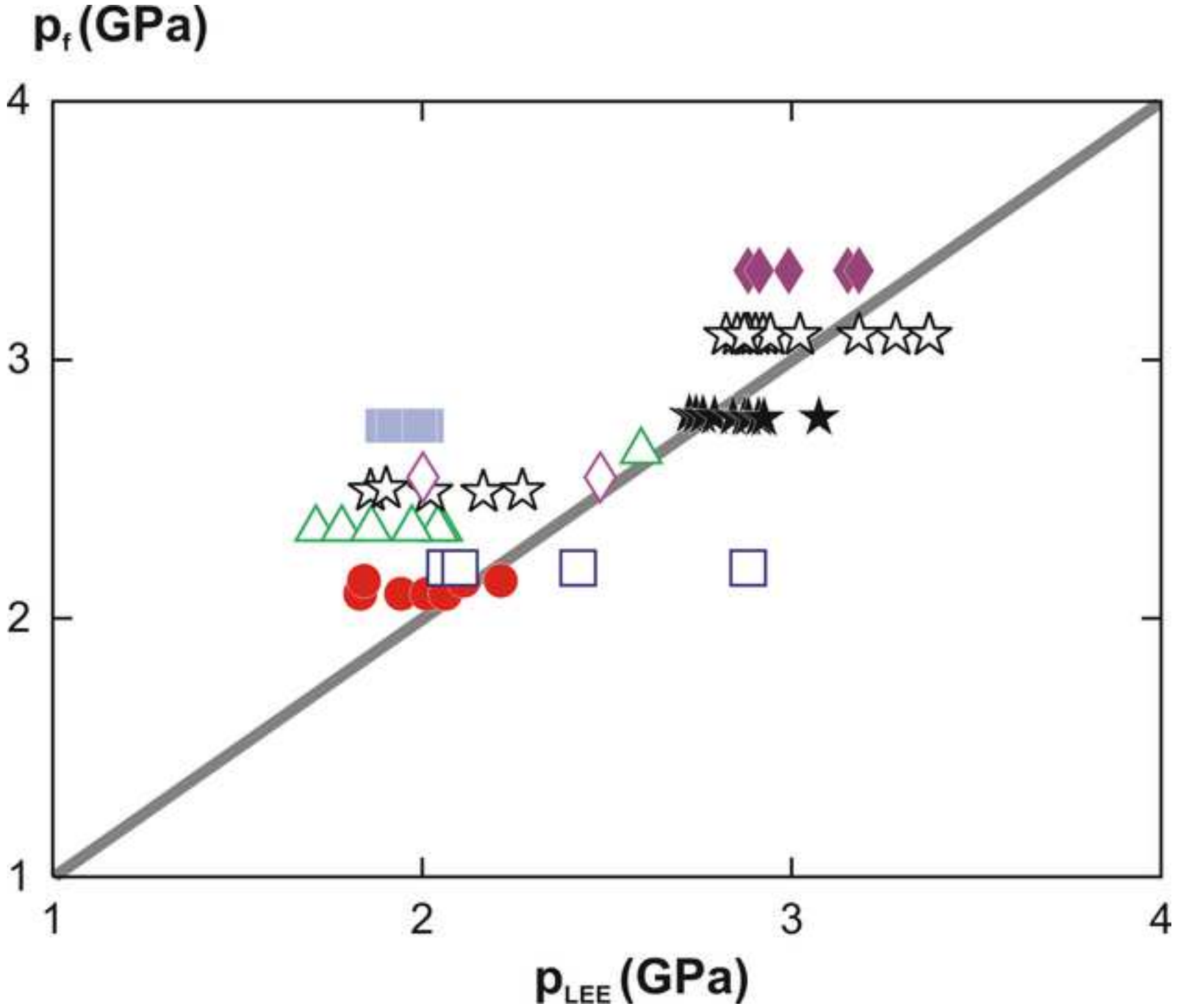

Figure 9
Click here to download high resolution image

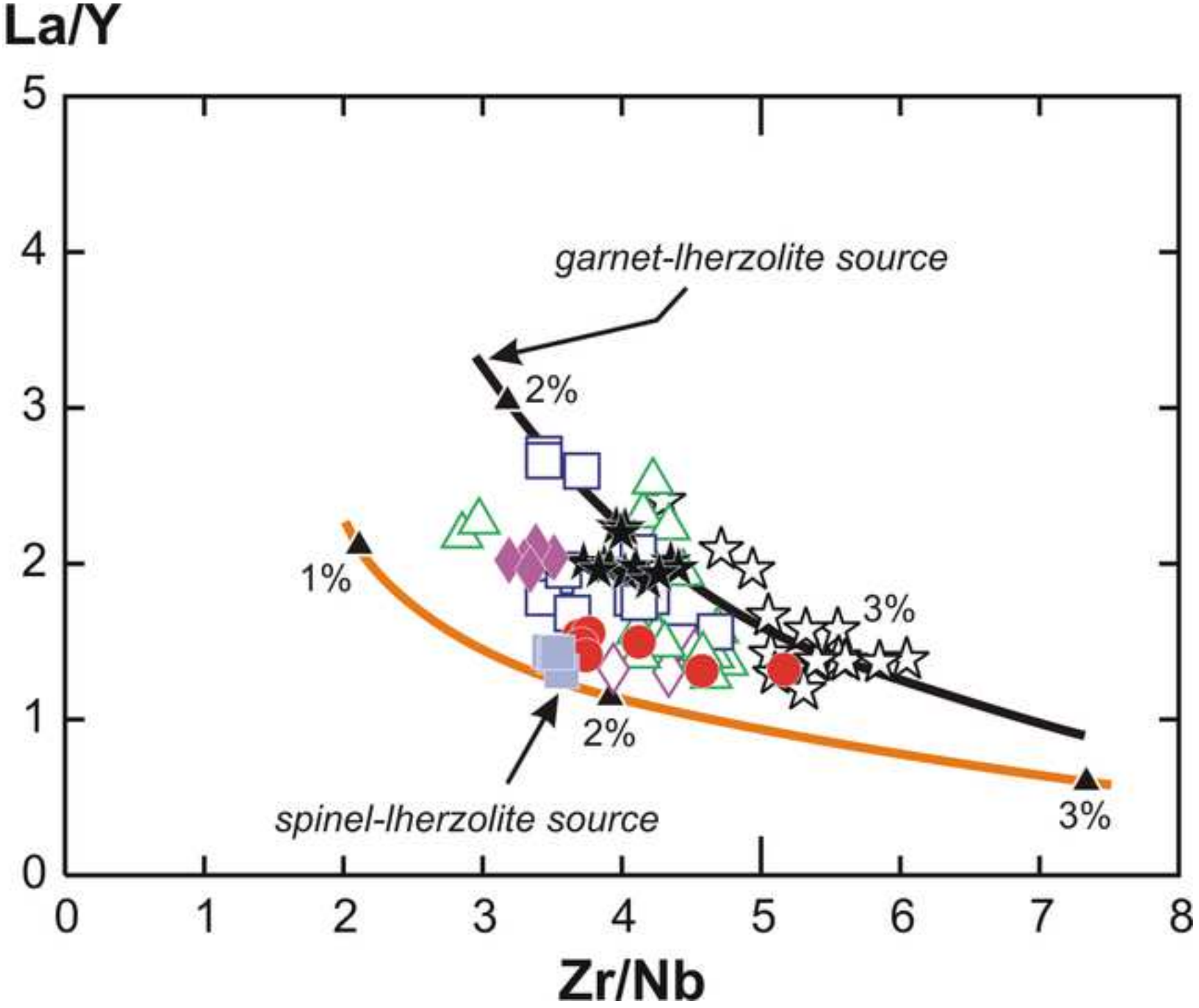

Figure 10
Click here to download high resolution image

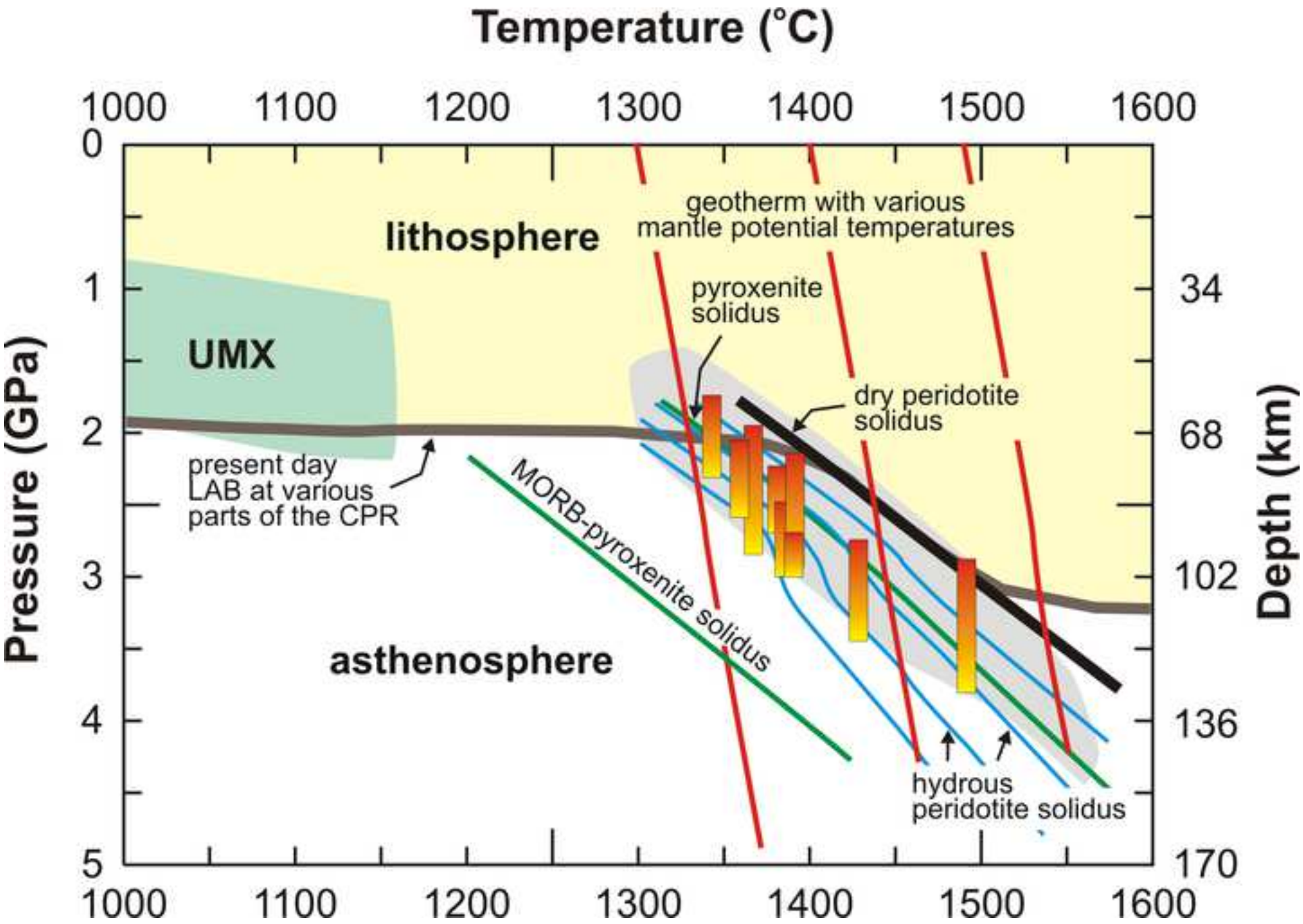

Figure 11
Click here to download high resolution image

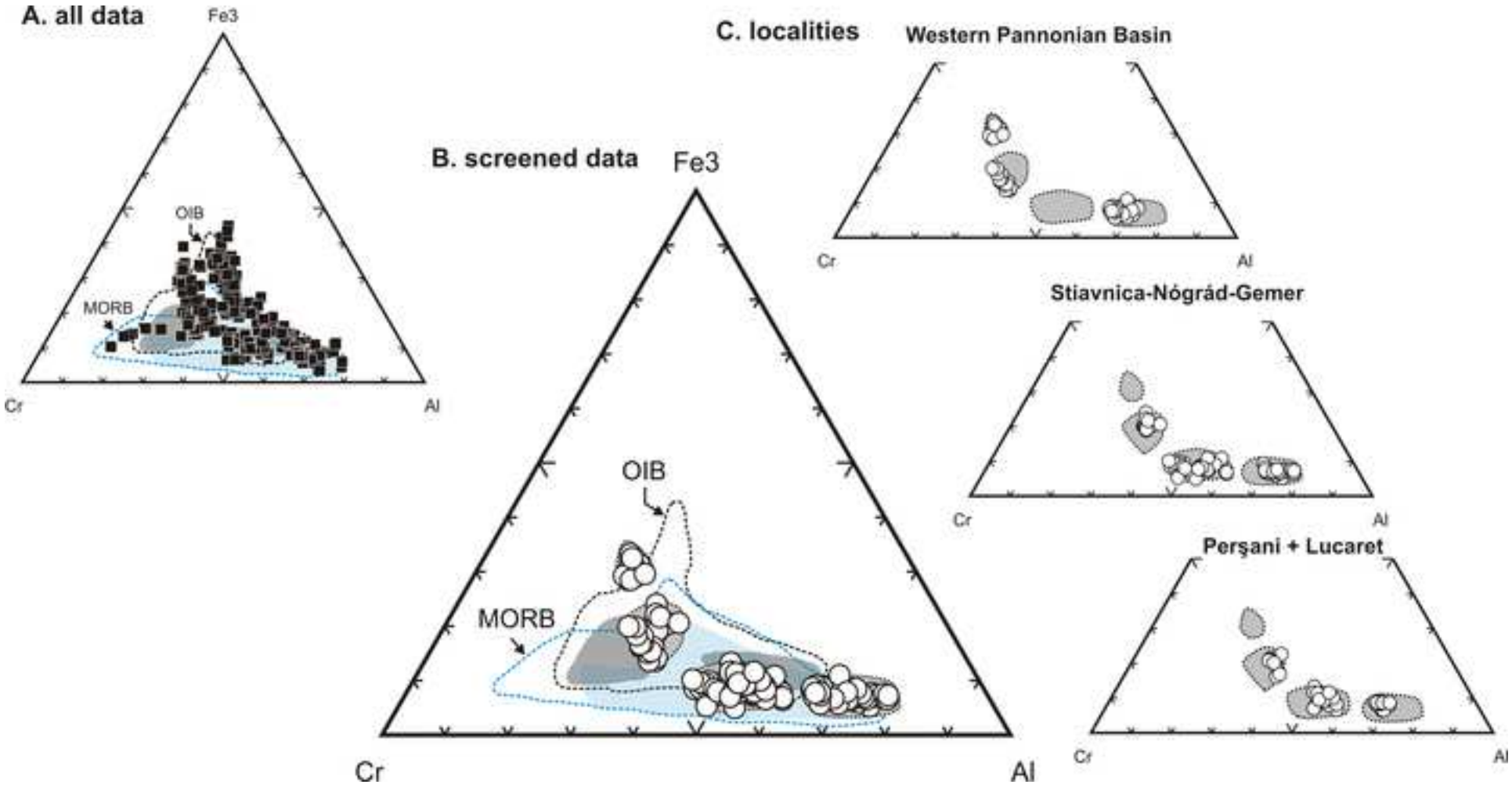

Figure 12
Click here to download high resolution image

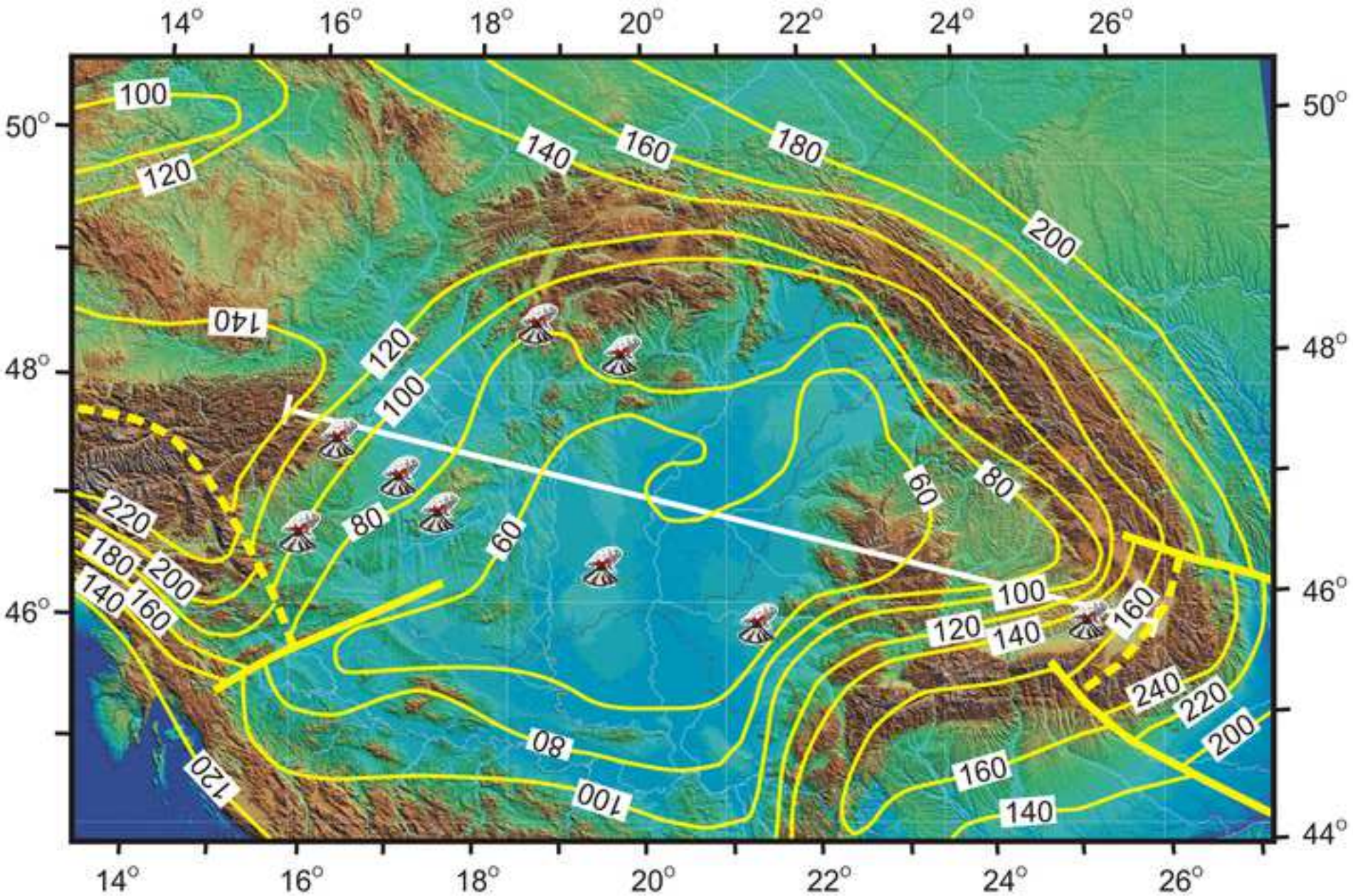

Figure 13
Click here to download high resolution image

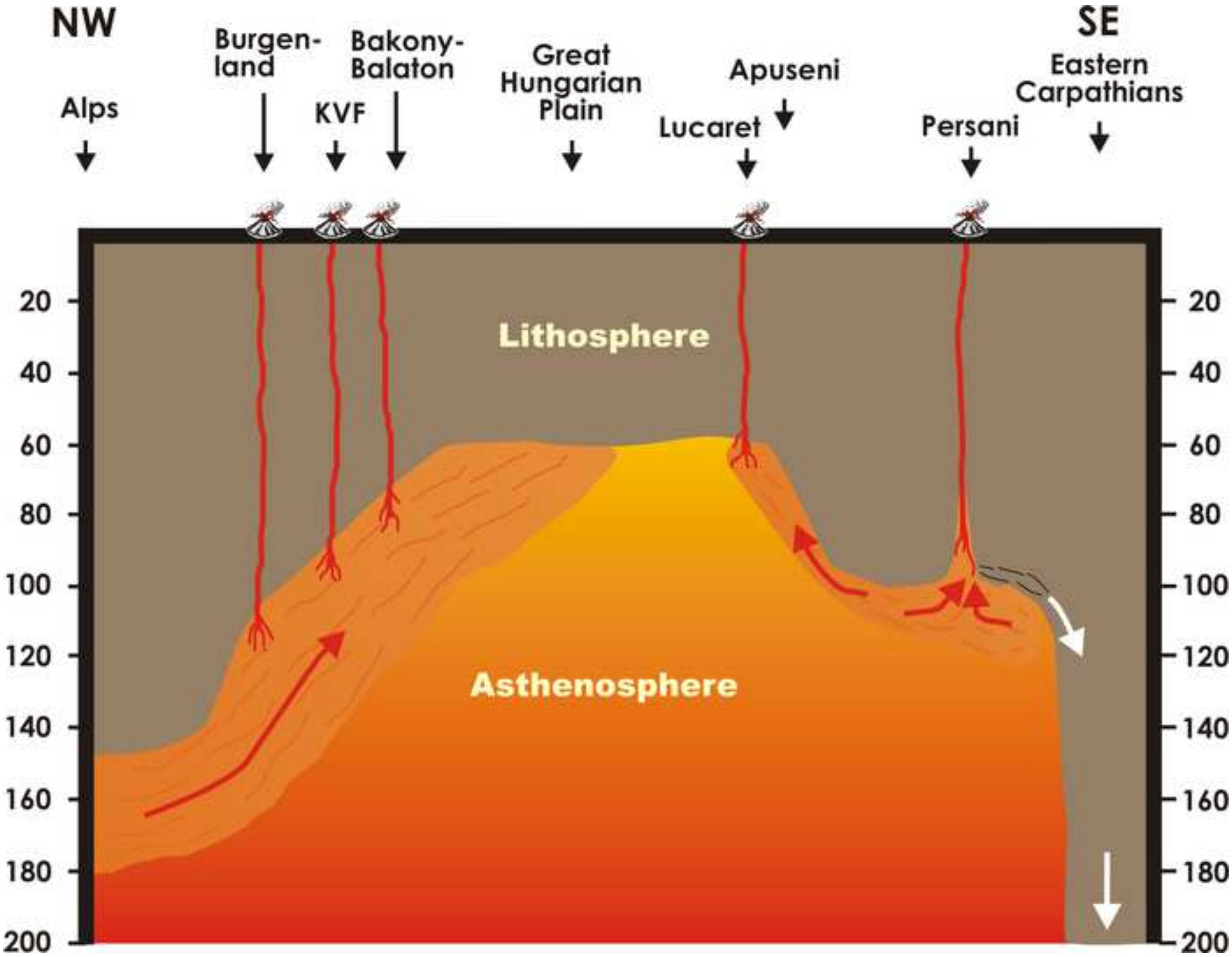

Table 1

sample	KL-4	ST-11	PLB-4	OB-1	SAG08-2	S-1	KK-1
locality	Klöch	Steinberg	Pauliberg	Oberpul-lendorf	Ság	Sátorma	Kapolcs
volcanic field	SVF	SVF	BU	BU	KVF	BBVF	BBVF
Reference	1	1	2	2	3	3	3
SiO2	44.97	43.87	46.99	49.07	48.19	47.24	46.53
TiO2	2.25	2.12	3.76	2.73	2.31	2.18	2.24
Al2O3	15.58	14.92	11.13	12.75	14.10	15.51	15.37
Fe2O3t	10.03	11.02	12.59	11.58	11.79	10.35	10.86
MnO	0.17	0.20	0.15	0.20	0.14	0.16	0.15
MgO	9.40	8.19	10.54	9.14	9.55	9.03	9.61
CaO	10.19	10.80	9.95	10.13	9.04	8.80	9.26
Na2O	4.58	5.47	2.78	2.65	2.83	3.65	3.13
K2O	2.11	2.37	1.48	1.31	1.53	2.30	2.18
P2O5	0.72	1.06	0.62	0.44	0.50	0.79	0.67
LOI	0.98	0.23	0.11	2.12	2.1	1.6	1.4
mg-number	0.69	0.63	0.66	0.65	0.65	0.67	0.67
S.I.	-27.25	-38.32	-3.19	2.40	-0.44	-12.19	-10.31
Ni	138	123	274	324	228	200	172
Cr	136	121	332	287	356	246	260
V	215	206	172	200	198	182	176
Sc	19.4	13.6	16.4	20.9	21	19	22
Co	38.1	36	51.5	45.6	48.7	41.4	41.4
Rb	52.8	62.2	39.8	21.2	26.5	56.8	50.7
Ba	581	713	479	305	602	877	627
Sr	1008	1203	881	577	808.1	1159.2	1385.8
Zr	368	556	498	364	187.8	282.9	194.7
Nb	94.2	111	72.4	49.8	40.9	80.1	53.3
Y	28.5	34.3	31.4	27.3	21.1	27.5	21.5
Th	9.9	12.6	5.26	3.64	4.7	8.8	6.7
La	56.6	75.4	43.4	25.9	29.8	52.9	36.2
Ce	104	135	94.8	64.2	59.8	101.3	72.1
Pr	11.4	14.5	12.1	6.9	7.81	12.2	9.11
Nd	46.2	59	49.7	30.7	31.6	48.7	37.8
Sm	7.26	8.97	10.5	6.16	6.87	8.13	6.69
Eu	2.24	2.71	3.07	1.92	2.13	2.36	2.05
Gd	6.68	8.09	9.2	5.82	5.86	6.76	5.67
Tb	0.87	1.02	1.23	0.806	0.85	0.8	0.73
Dy	4.45	5.15	5.89	4.11	4.37	4.86	4.22
Ho	0.82	0.94	1.04	0.755	0.74	0.84	0.78
Er	2.1	2.43	2.53	1.87	1.87	2.21	1.95
Tm	0.28	0.32	0.312	0.249	0.28	0.31	0.28
Yb	1.8	2.04	1.91	1.53	1.49	1.88	1.52
Lu	0.25	0.28	0.246	0.21	0.21	0.28	0.24
Hf	5.96	8.82	9.32	6.16	4.9	6	4.8
Ta	5.12	6.82	3.43	2.69	2.1	4.5	3.3
U	2.54	3.03	1.57	0.917	0.9	2.3	1.8
p_f	2.8		3.1	2.5	2.35	2.2	2.2
p_o	2.9		3.8	3.8	3	2.8	2.9
T	1390		1472	1416	1376	1343	

p	2.72	2.61	1.86	2.05	2.10

PUT-2	CSAM1	LU52	BARC
Putikov	Belinsky vrch	Lucaret	Barc
SE	NGVF	LU	PVF
3	3	3	4
44.32	48.43	48.90	46.82
2.53	1.94	2.23	1.78
13.64	15.07	14.45	16.01
12.11	10.91	10.82	10.16
0.19	0.16	0.15	0.17
11.32	10.03	8.54	9.26
10.62	7.82	8.58	9.48
2.91	3.86	4.00	3.93
1.32	1.45	1.76	1.92
1.04	0.32	0.57	0.48
2.4	0.2	-0.4	-0.1
0.69	0.68	0.65	0.68
-11.85	-6.60	-8.17	-16.11
238	234	138	179
383	191.5766	177	315
216	180	144	194
24	19	10.1	26
47.8	51.2	41.4	41.1
27.8	32	36	43.1
617	445	464	758
1011	684.5	627	775
262.9	152	183	185.3
82.6	38.5	51.4	51.8
23.8	19.4	22.6	23.8
6.2	3.3	4.72	6
48.1	25.8	29.5	32.8
93.4	48.9	60	63.9
11.35	5.57	7.61	7.59
46.9	22.5	31.5	34
8.65	4.6	7.12	6.04
2.49	1.48	2.23	1.86
6.86	4.42	6.28	5.14
0.83	0.71	0.94	0.7
4.91	3.92	4.92	4.35
0.8	0.7	0.94	0.83
1.99	1.91	2.38	2.26
0.27	0.27	0.31	0.34
1.6	1.65	2	2.21
0.22	0.24	0.28	0.31
5.6	3.6		4.5
4.8	2.4	2.85	3.1
2	0.8	1.35	1.7
3.35	2.55	2.75	2.15
3.6	3	3.2	2.6
1418	1386	1395	1378

2.91	2.00	1.99	2.21

Electronic Supplementary Material

Click here to download Electronic Supplementary Material: Supplementary_data.xlsx